CSIRO PUBLISHING

www.publish.csiro.au/journals/ijwf *International Journal of Wildland Fire* **2010**, *19*, 179–201

A numerical study of slope and fuel structure effects on coupled wildfire behaviour

Rodman R. Linn[A,D], *Judith L. Winterkamp*[A], *David R. Weise*[B] *and Carleton Edminster*[C]

[A]Earth and Environmental Sciences Division, Los Alamos National Laboratory, Los Alamos, NM 87545, USA.

[B]USDA Forest Service, Pacific Southwest Research Station, 4955 Canyon Crest Drive, Riverside, CA 92507, USA.

[C]USDA Forest Service, Rocky Mountain Research Station, 2500 S Pine Knoll Drive, Flagstaff, AZ 86001, USA.

[D]Corresponding author. Email: rrl@lanl.gov

Abstract. Slope and fuel structure are commonly accepted as major factors affecting the way wildfires behave. However, it is possible that slope affects fire differently depending on the fuel bed. Six FIRETEC simulations using three different fuel beds on flat and upslope topography were used to examine this possibility. Fuel beds resembling grass, chaparral, and ponderosa pine forests were created in such a way that there were two specific locations with identical local fuel beds located around them. These fuel beds were each used for a flat-terrain simulation and an idealised-hill simulation in order to isolate the impacts of the topography without the complications of having different local fuels. In these simulations, fuel bed characteristics have a significant effect on the spread rate and perimeter shape of the fires on both flat ground and on the idealised smooth hill topography. The analysis showed that these simulated fires evolved as they travelled between the locations even on flat ground, and the accelerations and decelerations that affect the fire occurred at different times and at different rates depending on the fuel bed. The results of these simulations and analyses indicate that though some general principles are true for all fuel beds, there are differences in the way that fires react to non-homogeneous topographies depending on the fuel bed.

Additional keywords: fire propagation, FIRETEC, non-local slope effects, vegetation structure effects.

Introduction

There is a continuing desire to understand wildland fires in order to make better decisions about how to protect lives and property, manage natural fuels, and assess risk. Various modelling approaches have been or are being used, from empirical formulations (Andrews 1986; Cohen 1986; Finney 1998), to approaches based on modelling some of the physical processes that drive wildfire (Dupuy and Larini 1999; Porterie *et al*. 2000; Grishin 2001*a*, 2001*b*; Margerit and Séro-Guillaume 2002; Séro-Guillaume and Margerit 2002; Dupuy and Morvan 2005; Koo *et al*. 2005; Mahalingam *et al*. 2005; Zhou *et al*. 2005, 2007; Mell *et al.* 2007), to combinations of the two (Clark *et al*. 1996, 2004; Bossert *et al*. 2000), to statistical models (Lindenmuth and Davis 1973; Weise *et al*. 2005) that predict spread rate or the probability that a fire will propagate at all in different types of chaparral. Other researchers use models to focus on particular phenomena, such as ignition of crown fuels in idealised circumstances (Cruz 2004).

An aspect of a model can be considered self-determining if that aspect does not have a predetermined value for a given set of fire-environment conditions and fire history. For instance, the spread of the fire is self-determining if the spread rates that simulated fires display are the result of a complex set of drivers that are independently intended to represent the processes that drive the fire but are not individually linked or calibrated to the spread rate. It is important to note that being considered self-determining does not make any statement about the accuracy of a model, but merely refers to the fact that the observable fire behaviours are not prescribed by the model explicitly. One of the strengths of models that have some self-determining characteristics (Dupuy and Larini 1999; Porterie *et al*. 2000; Grishin 2001*a*, 2001*b*; Margerit and Séro-Guillaume 2002; Séro-Guillaume and Margerit 2002; Dupuy and Morvan 2005; Koo *et al*. 2005; Mahalingam *et al*. 2005; Zhou *et al*. 2005, 2007; Mell *et al*. 2007) is that they can be used to suggest ways that observable fire behaviour like spread rate may be connected to underlying processes because they have not been specified explicitly.

It is widely recognised that fires often accelerate dramatically up a hill, all other things being equal. Thus, the impact of topography on aspects of fire behaviour including the rate and direction of spread, flame length, and fireline thickness has been studied by a variety of researchers. Some of this work has been experimental, such as the fire table studies done by Weise and Biging (1994), Dupuy (1997), and Viegas (2004*a*, 2004*b*). Other research in this area has focussed on modelling and explaining

 10.1071/WF07120 1049-8001/10/020179

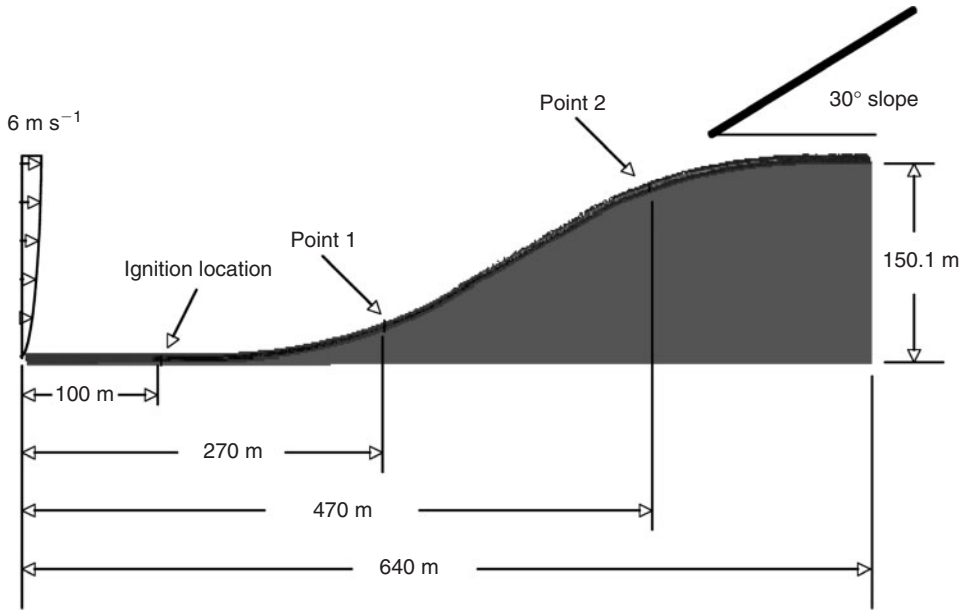

Fig. 1. Diagram showing the profile of the hill topography with locations of the fireline ignition, point 1, and point 2.

fire behaviour on slopes using empirical formulations, including the pioneering work of Byram *et al*. (1964) and Rothermel (1972), as well as later work by Nelson (2002) and Forthofer *et al*. (2003). Another modelling approach couples an empirical fire model or heat source with an atmospheric transport model to simulate wildfire behaviour on slopes, including work described in Heilman (1992), Reisner *et al*. (1998), and Coen (2000). In recent research, a physics-based wildfire model, FIRETEC, has been used to simulate wildfire behaviour in inhomogeneous topography and fuels (Linn *et al*. 2007).

HIGRAD/FIRETEC is a coupled atmospheric transport–wildfire behaviour model. Like some of the other transport-based models for fire behaviour (Dupuy and Morvan 2005; Mahalingam *et al*. 2005; Zhou *et al*. 2005, 2007; Mell *et al*. 2007), HIGRAD/FIRETEC is based on solving equations for the conservation of mass, momentum and energy, and capturing fine-scale processes through subgrid models. According to the interpretation of self-determining described above, HIGRAD/FIRETEC exhibits a variety of self-determining properties such as spread rate and fire shape. In addition, it is capable of simulating fires in three dimensions with complex topographies. The self-determining properties of this physics-based model provide the potential of capturing facets of the coupled fire–atmosphere–topography interaction.

Linn (1997) used a two-dimensional (vertical slice) version of FIRETEC to simulate fires in idealised uphill, downhill, and canyon topographies. A three-dimensional version of FIRETEC coupled with HIGRAD was later used to simulate fires in complex terrain, such as a portion of the Calabasas fire (Bossert *et al*. 2000) and hypothetical fires on real topography (Linn *et al*. 2002). These previous works show the potential value of exploring fire behaviour responses to topographic situations with different fuel beds using FIRETEC, even though this model is a work in progress where various simplifications and approximations have been made. For instance, the basic model that was most recently described in Linn and Cunningham (2005) and Colman and Linn (2007) uses a simplified mixing-limited combustion model and a diffusion-based radiation model that has been tailored for transport through optically thin media. In addition, the fact that the model resolutions are typically larger than one metre implies that subgrid models depending on averaged quantities, correlations of fluctuations and probability density functions must be used to capture the combined impacts of unresolved details.

For the current work, a set of simulations was performed using the HIGRAD/FIRETEC model. The goal of these simulations was to explore aspects of fire behaviour that can be directly linked to topography and non-local effects of topography.

Simulations

Six simulations were performed using FIRETEC, a physics-based wildfire model described in detail in Linn (1997), Linn *et al*. (2002, 2005), Linn and Cunningham (2005), and Colman and Linn (2007). These simulations were performed on either flat ground or on an idealised hill with a 30° slope so that the change in elevation was 150.1 m. Fig. 1 shows a profile of the hill topography, which has a flat section on the left of the domain, then a 30° incline that starts rising 140 m from the left edge of the domain and continues rising to 600 m from the left edge and then is level again at 150.1-m elevation.

The profile of this hill is produced by combining two similar sections of an ellipse (forming the rounded portions at the top and bottom of the hill) with a straight-line segment at 30° above horizontal from $x = 318$ to 422 m. The ellipse sections of the hill are designed to be tangential to the horizontal sections of

the profile at the top and bottom of the hill and tangential to the straight line in the middle of the slope that is 30° above horizontal. Fig. 1 also shows the x location of two points where simulation results will be compared.

Three different types of vegetation were used to populate the fuel bed for the entire domain on both the flat and hill topographies, resulting in six simulations. The first fuel bed was specified to be similar to tall grass of height 0.7 m, with a load of 0.7 kg m^{-2} and a fuel moisture fraction of 0.05 (kg water mass per kg dry fuel mass). This fuel is entirely contained within the first grid cell above the ground. Throughout the remainder of the paper, this fuel bed will be referred to simply as GRASS. The second fuel bed resembles the chaparral fuel complex found in California. The fuel bed was modelled with a 60% shrub cover composed of chamise (*Adenostoma fasciculatum* Hook. & Arn.) and ceanothus (*Ceanothus* sp.) with inhomogeneous grass and litter surface fuels. The maximum shrub height is 1.8 m, with an average bush diameter of 2.5 m and a canopy moisture fraction of 1.3 of the dry fuel mass. The canopy bulk density for these chaparral-like fuels is ~1.25 kg m^{-3} measured from the ground to the average shrub height of 1.6 m. For the remainder of this paper, this fuel type will be referred to as CHAP. The third fuel bed resembles a ponderosa pine forest (*Pinus ponderosa* P. & C. Lawson) with inhomogeneous grass and litter surface fuels. The fuel bed consists of representations of over 17 000 ponderosa pine trees that were generated using the methodology described in Linn *et al*. (2005). As in Linn *et al*. (2005), the discrete fuel elements used to model trees are based on data collected by the USDA Forest Service Rocky Mountain Research Station and Northern Arizona University as part of the Joint Fire Sciences Program, Fire and Fire Surrogate Treatment Project. The canopy bulk density over the forested area is ~0.24 kg m^{-3}, with an average tree height of 13.8 m (minimum of 7.3 m, maximum of 19.9 m) and an average height to live crown of 8.7 m (minimum of 3.9 m, maximum of 13.4 m). The canopy moisture fraction is 0.80 of the dry fuel mass. Throughout this paper, this type of vegetation will be referred to as PINE. For all three fuel beds, the surface area per unit fuel volume was estimated to be 4000 m^{-1}.

In order to provide a random but identical fuel bed at several different locations on the topographies, an 80 × 80-m inset fuel bed was generated using the methodologies described above for each of the GRASS, CHAP, and PINE fuel types. These inset fuel beds were created in such a way as to be symmetric about their streamwise centreline in order to facilitate other future studies. These 80 × 80-m fuel beds were then inserted at two locations, thus replacing the random placement of shrubs or trees in this region with an identical fuel bed at each location. This method of creating two identical fuel plots in the domain was used in order to eliminate the added complexity of comparing two locations with different local fuel structures. One inset fuel bed replaced the existing fuel bed at $x = 210$ to 290 m and $y = 120$ to 200 m, the other between $x = 410$ and 490 m and $y = 120$ and 200 m. These inset fuel beds are highlighted in Fig. 2*a*. Fig. 2*b* illustrates the fuel bed structure in the PINE canopy in the inset at a height of 11 m above the ground. In Fig. 2*b*, several computational cells are highlighted for the discussions below. The locations that are marked points 1, 1b, 2, and 2b are the locations in the inset fuel bed where detailed descriptions will be provided below, with 1 and 1b being in the left inset shown in Fig. 2*a* and points 2 and 2b

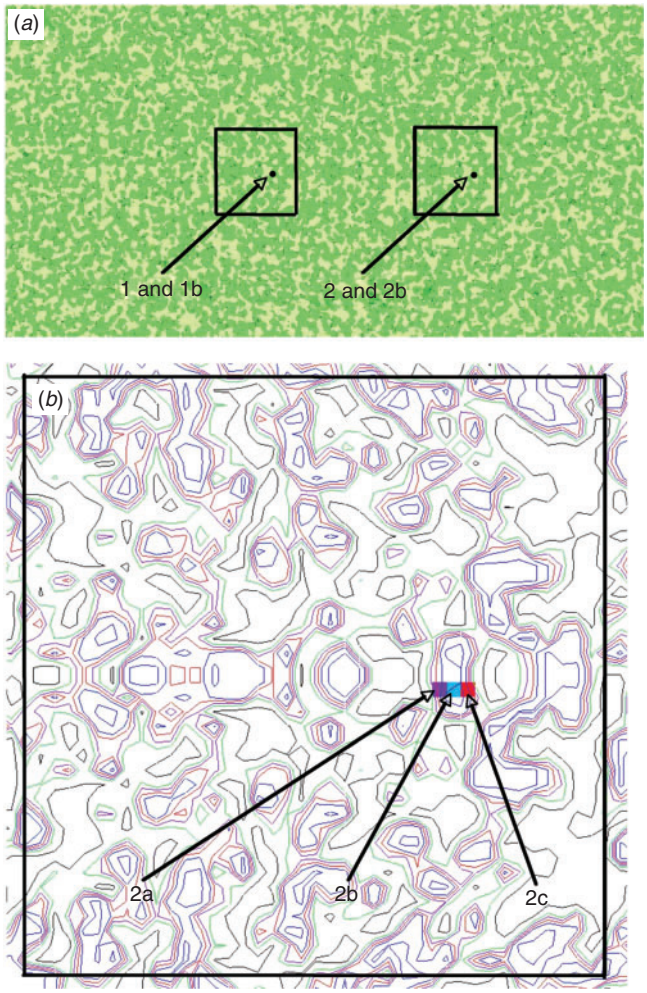

Fig. 2. Description of the PINE fuel bed: (*a*) shows a top-down view of the entire domain with the inset fuel beds outlined by the black boxes; (*b*) shows contours of the fuel density in the PINE inset fuel bed at $z = 11$ m with points 2a, b, and c highlighted.

in the right inset. Points 1 and 1b are located near the bottom of the hill and points 2 and 2b are near the top of the hill when the hill topography is used, as shown in Fig. 1. The difference between point 1 and point 1b is that point 1 is 0.7 m above the ground and point 1b is 11 m above the ground at this location. Similarly, point 2 is near ground level and point 2b is 11 m above it.

As mentioned above, an effort was made to eliminate the impacts of local fuel differences of the sorts described in Linn *et al*. (2005) in order to compare fire behaviour at points of interest within the inset fuel bed with fewer complicating factors. By placing the same tree or shrub arrangement at the lower part of the hill and at the upper part of the hill at locations with the same slope, we attempt to focus on effects of the evolution of the fire itself as it progresses on flat ground or on the hill. This approach is valuable, but does not provide a sense of the variability of behaviour within the stand. For this reason, we chose two additional locations, 2a and 2c, which are 2 m downwind and 2 m upwind of point 2b. These points are shown in Fig. 2*b*, which locates the points on contours of fuel bulk density 11 m above the ground.

The domain of the simulations is 640 × 320 × ~900 m. The horizontal grid spacing is 2 m, and the vertical grid spacing is ~1.5 m near the ground. The winds are initialised with a wind profile that was pregenerated by running HIGRAD/FIRETEC with an ambient 6-m s^{-1} wind and cyclic boundaries on flat topography so that a vertical shear profile develops near the ground owing to the drag associated with the vegetation. This wind profile is mapped onto the topography in order to provide an estimated profile for purposes of inlet conditions. The winds are then allowed to adjust for 200 s before the fire is ignited. The fire is ignited 100 m from the inlet wind source with a crosswind length of 100 m. The fires are ignited by raising the temperature of the ignition region from 300 to 1000 K over 4 s. The time step in these simulations is 0.01 s with subcycling on portions of the physics.

Spread rates and patterns

Spread rate and fire shape are two characteristics of wildfire behaviour that are affected by slope and fuel structure. Fig. 3 contains images from the six simulations that show the relative shapes of the fires around 470 m. Fig. 4 illustrates the fire shapes in each of the simulations using black lines to indicate the contours of the locations where the fuel is 50% consumed and red lines to indicate the contours of areas where the solid temperature is 500 K. Fig. 4*a–d* shows contours associated with the values in the cell closest to the ground for grass and chaparral on flat terrain and on the hill profile. Fig. 4*e–f* shows the contours in the cell closest to the ground in black and red as well as green lines to indicate the contours of the locations where the fuel is 50% consumed and blue lines to indicate the contours of areas where the solid temperature is 500 K at $z = 11$ m from the ground for PINEFLAT and PINEHILL. These images were created at times when the ground fires were burning approximately over point 2 ($x = 470$ m) at 270 s for Figs 3*a* and 4*a* (GRASSFLAT); 200 s for Figs 3*b* and 4*b* (GRASSHILL); 650 s for Figs 3*c* and 4*c* (CHAPFLAT); 430 s for Figs 3*d* and 4*d* (CHAPHILL); 565 s for Figs 3*e* and 4*e* (PINEFLAT); and 380 s for Figs 3*f* and 4*f* (PINEHILL).

Figs 3 and 4 illustrate that both the fuel structure and slope affect the spread rate and shape of the fire. All three fuel beds exhibit similar differences in the fire perimeter between the fires on flat terrain and on the hill topography. The shapes of the fire perimeters on flat ground (seen in Figs 3*a*, *c*, *e* and 4*a*, *c*, *e*) have some elliptical or ovoid-shaped features to them, even though these fires have not burned sufficiently far for the source to lose the signs of the straight-line ignition pattern. It should be recognised that the shape of the head fire on GRASSFLAT is more rounded than the shapes seen in Cheney *et al*. (1993). This is attributed to an interesting artefact of the simultaneous 100-m ignition in these simulations compared with the more practical method used in Cheney *et al*. (1993) where the grass fire is ignited by two men walking away from a central point. An ignition process designed to reproduce the experimental ignition method produces a more rounded head fire soon after ignition due to the fact that by the time the ends of the lines are ignited, the middle of the fire has already propagated a noticeable distance (depending on the wind speed and speed of the men walking). The simultaneous and instantaneous ignition was used in these simulations in order to simplify the process and allow for the shape of the head fire to be completely attributable to the spread rates. Previous researchers have studied these elliptical or ovoid characteristics, including Fons (1946) and Anderson (1983), and numerous operational fire behaviour models have been based on assumptions regarding the elliptical nature of fire spread, including FARSITE (Finney 1998), the Canadian Fire Behaviour Prediction System (Forestry Canada Fire Danger Group 1992), and Richards (1990). The shape of the fire front on flat ground is more rounded than when it is progressing up the hill (seen in Figs 3*b*, *d*, *f* and 4*b*, *d*, *f*). This effect has been documented in Dupuy (1997) and was described in Linn *et al*. (2007). Some of the fundamental phenomena that contribute to this feature (illustrated in several places later in the paper) are that the topography raises the head fire above the positions of the upwind ground, fuel, and burning zones. This raised position provides better ventilation to the head fire from the ambient wind, which not only makes the fire move faster but also changes the shape of the fireline. On flat ground, the wind arriving at the head fire is being affected by the entrainment of the flanking portions of the fire, whereas this competition is reduced when the fire is on a slope. Another key feature is the fact that the trajectory of the buoyant gases rising from the fireline has some component that is aligned with the indraft of the upslope portions of the fire, and so hot gases are entrained into the indraft of the upslope portion of the fire. The net effect of this behaviour is to funnel heat up the fireline until it reaches the head fire. The sharper the point of the heading fireline becomes, the more its upwind entrainment comprises heated gases from its downslope neighbours. The smaller angle of the rising hot gases from the ground inhibits the entrainment on the upslope side and accentuates the entrainment from the other side, thus driving the fire faster and making it more difficult to spread laterally. Another factor evident in these simulations is that as the fire shape narrows, one side of the fireline pulls on the other side of the fireline through its entrainment forces. This further narrows the fire shape and puts more heat into the air that eventually reaches the head fire.

From these figures, it is also clear that the fire has moved farther downwind in the simulations with the hill than the simulations on flat terrain for the same fuel type. Numerous researchers have observed this effect, including Fons (1946), Weise (1993), and Viegas (2004*a*). In addition, it can be noted that the thickness of the firelines differs for the different fuel beds in the simulations. For this purpose, we are referring to the thickness as a distance between the 500-K temperature contours. For example, the fireline thickness for the grass and chaparral fuel simulations is much thicker than for the pine simulation.

The evolving heading fire spread of the six simulated fires is illustrated in Fig. 5 by plotting the furthest downwind location where the resolved solid temperature is above 500 K. This location is a marker that is near the fire front. The changing slope of these lines, which are produced using output from the simulations every second, represents the evolution of the spread rate with time.

Fig. 5 illustrates that both of the grass fires spread faster than any of the pine or chaparral fires. The sharpest bends in the propagation curves (indicating acceleration and deceleration) are in the PINEHILL simulation. Additional simulations with various bulk densities, moistures, and surface area per

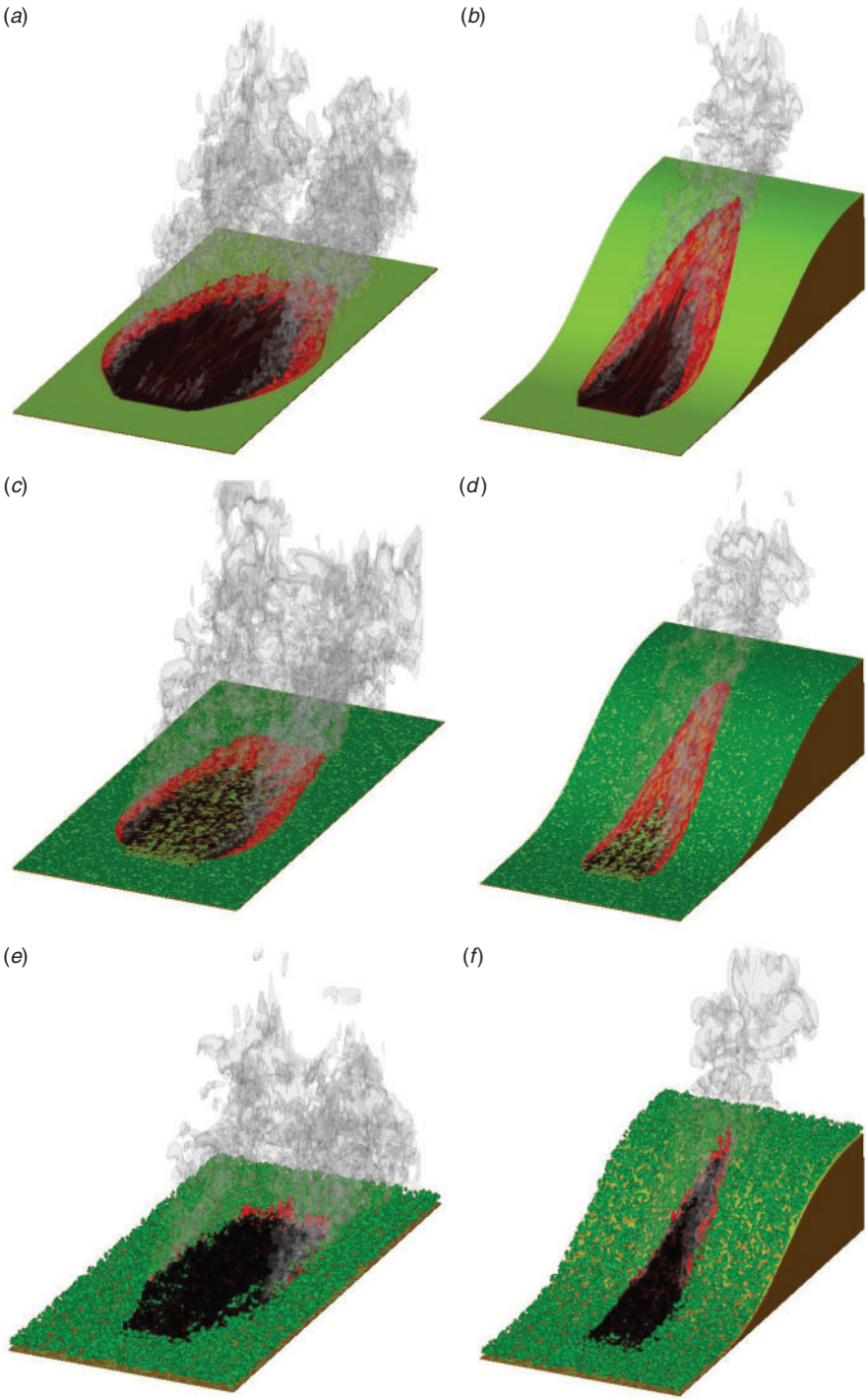

Fig. 3. Isometric images of fires on (*a*) GRASSFLAT; (*b*) GRASSHILL; (*c*) CHAPFLAT; (*d*) CHAPHILL; (*e*) PINEFLAT; and (*f*) PINEHILL as the fire reaches ~470 m. Dark, medium, and light green isosurfaces indicate locations of canopy fuels and grass; black and brown colours indicate locations where these fuels have been depleted. Red isosurfaces indicate hot gases.

unit volume characteristics for the fuel could be used to create families of curves for spread rate as a function of fuel characteristics. This is outside of the scope of this text, as the current focus is to explore some of the differences in processes controlling the simulated fire behaviour for various fuels and topographies.

The average spread rates over 20-m distances centred at five different locations in the domain are provided in Table 1. The

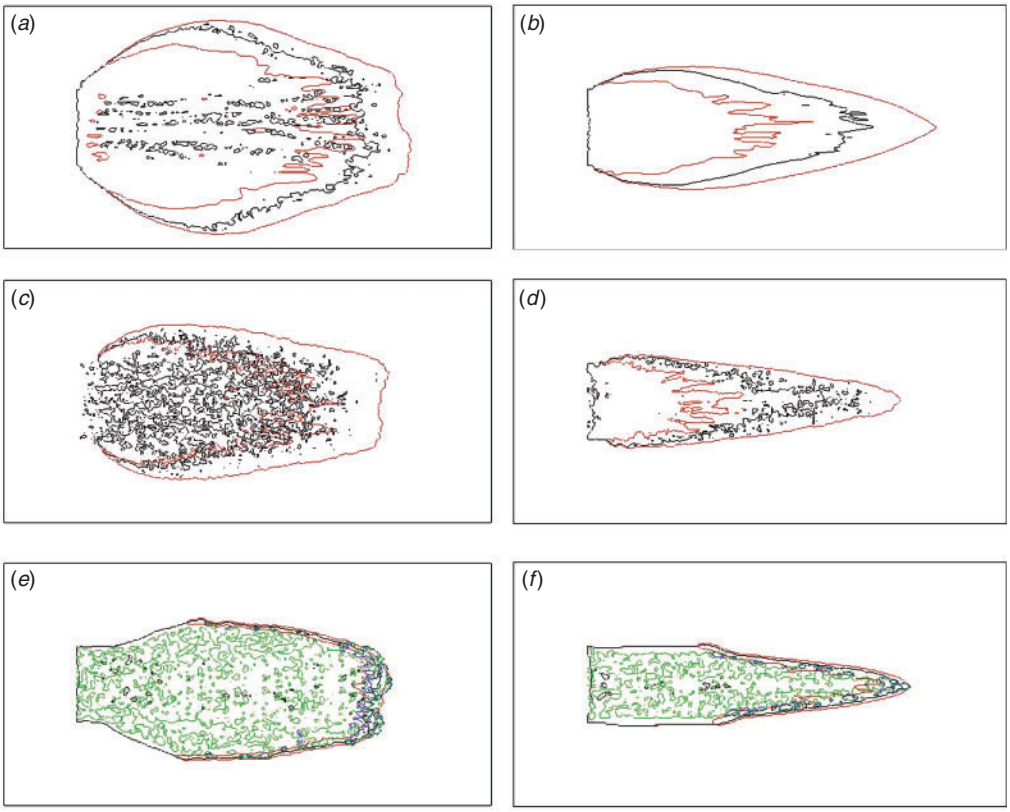

Fig. 4. Contour plots showing areas where 50% of the ground fuel is consumed using black lines, and areas where the solid temperature of the ground fuel is 500 K using red lines. Images (*e*) and (*f*) also show areas of 50% consumption and 500 K for the canopy fuels using green lines and blue lines. The simulations shown are (*a*) GRASSFLAT; (*b*) GRASSHILL; (*c*) CHAPFLAT; (*d*) CHAPHILL; (*e*) PINEFLAT; and (*f*) PINEHILL.

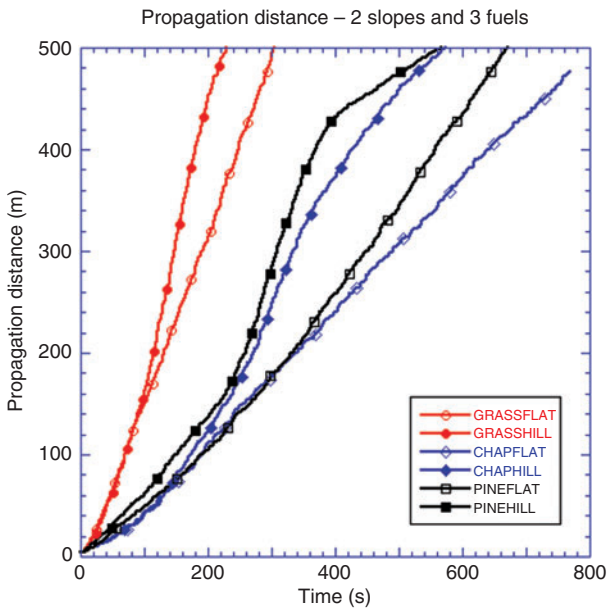

Fig. 5. Plot of downwind propagation distance as a function of time for simulated fires in grass, chaparral, and pine fuel beds for flat and hill topographies. The lines are generated by finding the farthest downwind location where the solid temperature is greater than 500 K at a frequency of once per second. The symbols are placed every 10 points.

locations chosen are symmetrically spaced around the centre of the slope. Therefore, when looking at the rows associated with the HILL topography, the columns of the same shade of grey have the same slope. The average slope of the topography over 20 m centred at $x = 170$ and 570 m is 0.074 (an angle of 4°), at point 1 and point 2 is 0.366 (an angle of 20°), and at $x = 370$ m is 0.58 (an angle of 30°). The hill topography simulations for all three fuel beds show an increase in spread rate when the fire is on the slope and a decrease in spread rate when the fire returns to flat ground at the top of the hill. The values in Table 1 illustrate several things for these simulations: (1) upslope topography eventually increases the spread rate of the fire in all fuel beds over what it would be on flat ground, but the rate at which the slope affects the spread rate is different for different fuels; (2) for the same local slope, local fuel load, fuel moisture, and high-level wind field, the spread rates are not the same at different places on the hill; (3) the coupled effects of slope and position on the slope affect fires with different fuels differently. For example, for the GRASSHILL and PINEHILL fires, the spread rate at point 2 is greater than the spread rate at point 1, whereas the CHAPHILL fire is slower at point 2 than at point 1. All of the HILL simulations show slower propagation at $x = 570$ m than at $x = 170$ m. The change in velocity between the bottom of the hill and the top of the hill is greatest in the PINE simulations. Fig. 5 shows that the PINEFLAT simulation continues to nominally accelerate during the course of the simulation (even though the value at 570 m in Table 1 shows a decrease in speed associated with a

temporary fluctuation in the slope of the propagation curve). This seems to be due to the fact that the fireline thickness is growing slowly. Another possible contributor to the fact that the PINEFLAT simulation continues to slowly accelerate is that there is a growing hole in the canopy for the ambient winds to penetrate down to the ground fire and feed the underside of the canopy fire. Through this process, it is also possible that there are a greater number of large resolved turbulence structures entrained behind the burning region into the hole of burned out vegetation. At some point, we expect that a balance will be achieved between the buoyancy of the fire and the indrafts behind the fire, so the fire would quit accelerating.

To better understand some of the simulated processes that lead to the differences in fire behaviour for the various fuel structures and topography, we have selected a set of points that are labelled in Figs 1 and 2. At each of these points, a set of computed values is extracted and plotted as functions of time in subsequent figures. These plots, which are similar in format to those used in Cunningham and Linn (2007), are a way to illustrate the evolution and interaction of some of the processes occurring at a single location because they allow the reader to observe the relative timing and magnitude of various events. These plots contain a lot of information, and thus it is not possible to describe all of the interactions that are illustrated in this text. We will describe some of the interactions or behaviours in the following section.

Comparison of understorey fires

Two types of plots are presented in Fig. 6. One type of plot illustrates the evolution of solid-fuel temperature and the three components of the wind velocities parallel to the x, y, and z direction at a point. In these plots, we will refer to the times when the solid temperature is above 400 K as 'active burning'. The other type of plot shows the evolution of the net convective and net radiative heat flux of the fuel, as well as the evolution of the normalised amounts of solid fuel, water and oxygen, expressed as a fraction of the initial conditions. It should be noted that although these plots are very similar to those presented in Cunningham and Linn (2007), these net convective and radiative heat fluxes (energy per unit surface area of the fuel per unit time) are not directly comparable with the net convective and radiative heating values that were shown in that paper (energy per unit bulk volume per unit time). Cunningham and Linn's (2007) results can be converted to match the form of the heat fluxes presented here by dividing the bulk volume heating values by the surface area of the fuel per unit bulk volume of the fuel. These values are being presented in this fashion in order to be in the form of a usual heat flux (per unit area). This form also effectively accounts for the amount of fuel that is left in a cell. The presentation method used in Cunningham and Linn (2007) showed the heat transfer to the fuel falling owing to the depletion of the fuel and might mask the actual heat flux per unit of fuel surface area. The net convective heat and net radiative heat fluxes represent the heat flux absorbed minus the heat flux emitted from the fuel. The outputs from the simulations were generated every second for these plots so that oscillations of frequency greater than ~1 Hz are not shown. In addition, turbulence with length scales smaller than ~3 m is not resolved, and the energy associated with these smaller scales is captured by the turbulent kinetic energy (see Linn and Cunningham (2005) for details).

Ground fire behaviour for GRASS fuel on FLAT topography

In order to assess the impact of topography on the variation in the evolution of processes as a fire burns over a location, it is important to first understand how much variation occurs from one point to another within the same fuel bed on flat terrain. Fig. 6 contains four plots that illustrate the evolution of properties and processes at points 1 and 2 for GRASSFLAT in the cell that is nearest the ground. In order to interpret these plots, it is important to remember that the left side of the plot indicates the time when the fire has not yet reached the point and the right side of the plot represents a time after the most intense burning has passed.

It should be emphasised that we are very interested in the relationships between the properties and their coupling, but the significance of the precise magnitudes of these values should be considered as providing topics for future research or a direction for future experimental measurements. These values have not been validated against field data for these specific wind, topography and fuel scenarios, and the simulations show that a single measurement in a fire might not be representative of the value at other locations because there is a lot of variability even along the centreline of a fire in a homogeneous fuel bed. Simulated results have been compared with experimental data for various scenarios (Bossert *et al*. 2000; Bradley 2002; Linn and Cunningham 2005; Linn *et al*. 2005) with favourable results in terms of fuel consumption patterns, spread rates and patterns as well as characteristics of fire behaviour that are driven by coupled fire–atmosphere behaviour. From these comparisons, it is believed that FIRETEC simulation results have the capacity to capture some realistic facets of fire behaviour. The following figures represent one combination of processes that lead to simulated fire behaviour with FIRETEC. There might be other combinations that work as well, but these are the ones that this model produced for these idealised situations.

It is important to recognise that the values shown in the plots like Fig. 6 are cell-averaged values. In other words, FIRETEC cannot predict the evolution of temperature or moisture content for a single pine needle or leaf. There is an attempt to account for the impact of the subgrid variations using probability distribution functions and mass-weighted averaging as described in Linn (1997) and Linn and Cunningham (2005). The result of this representation of the physics is that, for instance, moisture begins to evaporate well before the average temperature of the fuel is at the boiling point and continues well after the average temperature has risen past the boiling point.

In Fig. 6*a*, *b*, the evolution of the average solid temperature and three velocity components (u, streamwise; v, crosswind; and w, vertical velocities) is shown as a function of time for the GRASSFLAT simulation at points 1 and 2. In both of these plots, there is a strong negative pulse of u velocity as the solid temperatures begin to rise, indicating an indraft in front of the fire that is contrary to the ambient winds. This indraft is a combination of crosswind vorticity and a seam between two counter-rotating vertical vortices. The u winds after the fire has passed are significantly greater than those that were present even 40 s before

Table 1. Spread rates averaged over 20-m distances that are centred at five different locations in the domain
The columns of the same shade of grey have the same slope. The slope of the topography at the points at $x = 170$ and 570 m is 0.074 (an angle of 4°), at point 1 and point 2 is 0.366 (an angle of 20°), and at $x = 370$ m is 0.58 (an angle of 30°)

Simulation	Spread rate ($m\,s^{-1}$)				
	$x = 170$ m	$x = 270$ m, point 1	$x = 370$ m	$x = 470$ m, point 2	$x = 570$ m
GRASSFLAT	1.8	1.7	1.6	1.5	1.7
GRASSHILL	2.3	2.6	3.0	3.0	1.7
CHAPFLAT	0.63	0.57	0.72	0.71	0.69
CHAPHILL	0.62	1.1	1.45	0.87	0.58
PINEFLAT	0.51	1.0	1.0	1.1	0.87
PINEHILL	0.78	1.2	1.9	1.7	0.40

the fire arrived. This elevated velocity results from the indraft of the fire augmented by the ambient wind that is no longer subject to as much drag because the fire has burned off the fuel. The *v* and *w* winds at both point 1 and point 2 fall back to nearly zero after the fire has passed, which is not unexpected as points 1 and 2 are very close to the centreline of the fire and the inlet velocity is steady and perfectly aligned with the *x*-axis. The solid temperatures at both locations reach ~1200 K.

The differences between the curves on these two plots are indicative of a combination of the evolving conditions of the fire and the temporal intermittency and spatial heterogeneity of the fire. For example, the duration of the high temperature is significantly longer at point 2 (Fig. 6*b*) than point 1 (Fig. 6*a*). The connection to the spatial heterogeneity is illustrated with contours of 500-K solid temperature at times 165 and 285 s in Fig. 7*a*, *b* for the FLATGRASS simulation. These times are ~45 s after the onset of the active burning, but the temperature is down to ~500 K at point 1 and still above 1000 K at point 2.

Points 1 and 2 are labelled on Fig. 7*a*, *b*, and show the fact that point 1 lies very near the 500-K contour that outlines one of the fingers of residual heat behind the fireline. Point 2 is in the middle of one of the fingers of residual heat, therefore staying hot much longer. Other notable differences between these two graphs are the larger period and amplitude of the fluctuations in the *u*-velocity during and after the active burning period. The velocity fluctuations in Fig. 6*b*, as well as the *v*- and *w*-components, are associated with resolved turbulent structures that are larger at point 2 than at point 1 in the GRASSFLAT simulation. These structures are likely to be associated with the non-homogeneous fireline structure seen in Fig. 7*b*. This structure is a result of tilted counter-rotating vortices (vertical vortices leaned forward) and is described in detail in Linn and Cunningham (2005).

Fig. 6*c*, *d* illustrates the evolution of the convective and radiative heat flux as well as the normalised solid fuel mass, water mass, and oxygen concentration at points 1 and 2. Some general trends can be seen in both plots, including slow radiative preheating with a weak convective cooling response as the fire approaches the points. During this time, the moisture is beginning to evaporate and the oxygen concentration begins to drop. The fact that the oxygen concentration drops before active burning begins indicates the gases blowing over the points at that time have passed in the vicinity of an upwind flame or through the plume where oxygen has already been depleted. As the fire gets very close to the two points, the convective and radiative fluxes to the fuel increase significantly, causing the reaction rate to rise quickly and fuel to begin to be depleted.

It is worth noting that the radiative heat absorbed by the fuel comes from a combination of hot solid sources and hot gas sources. As the burning area approaches the points, the radiation from the solid emitters increases, but there are also intermittent pulses of increased radiative heating that are due to radiating gases that sweep over the point. When the radiative flux is increased by the intermittent pockets of hot radiating gases that momentarily surround the point, the increases in radiative heat flux occur at the same time as increases in convective heat transfer, such as that seen in Fig. 6*c* at ~120 s.

This point in time, which is the onset of active burning, is at the same time as the strong rise in the temperatures and the reversed *u* velocity pulses that were seen in Fig. 6*a*, *b*. In the GRASSFLAT simulation, as soon as the temperature rises above ~900 K, the convective and radiative fluxes start to decline and the convective heat flux quickly becomes negative owing to the fact that the gas temperature is less than the solid temperature. The oscillations in the convective heat transfer patterns are strongly tied to the velocity fluctuations mentioned above; however, this is also complicated by the fact that convection is driven by the difference between solid and gas temperatures. During the most intense burning period, the convective cooling flux at point 1 has strong perturbations of $\pm 25\,kW\,m^{-2}$, whereas the perturbations in the convective cooling flux at point 2 are much smaller at $\pm 5\,kW\,m^{-2}$. This difference is interesting considering the scales and magnitude of the resolved turbulence are much larger at point 2. In fact, the spatial heterogeneity of the burn pattern contributes to the lower magnitude and fluctuation amplitude at point 2 because the gases have heated considerably over the tail of the heated area seen in Fig. 7*b*.

The increase in convective cooling near the tail of the heated region occurs because the gases reaching point 1 or point 2 at that time have not had a chance to be heated as they have not travelled over the heated ground. In particular, one of the strong convective cooling pulses at point 2 is associated with the large negative *v*-velocity fluctuations at 290 s. This fluctuation is a pulse of air coming from the side of the heated fuel finger and is pulled in by the indraft from the rising air seen at that time. The radiation eventually becomes negative in these simulations, but it is more complex owing to the fact that the radiative flux to the fuel is the sum of the energy absorbed from surrounding hot fuels

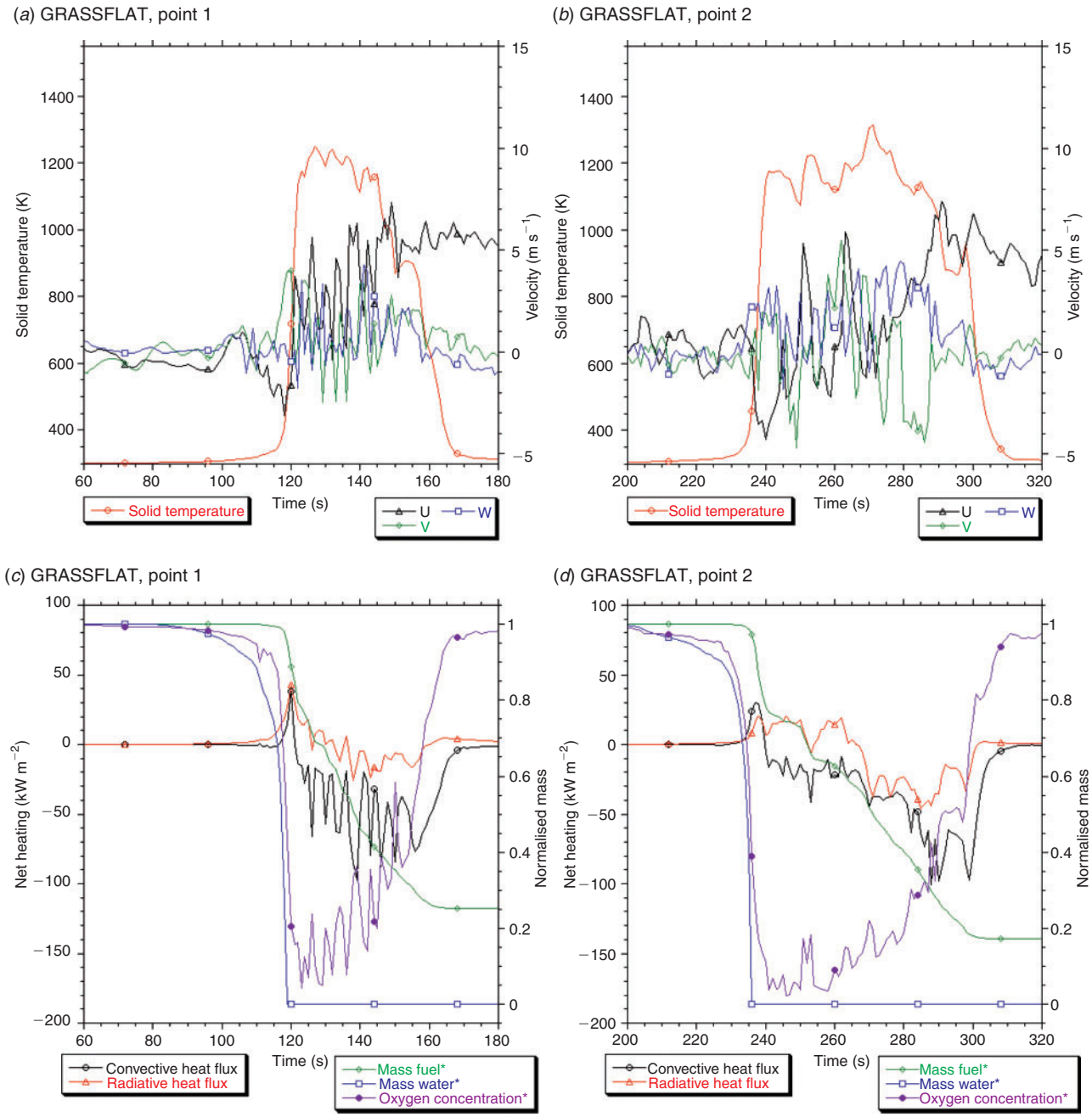

Fig. 6. Time series of quantities from the GRASSFLAT simulation. Solid fuel temperature (red line), u or streamwise (black line), v or crosswind (green line), and w or vertical (blue line) components of the wind velocity at (*a*) $x = 270$ m for point 1; and (*b*) $x = 470$ m for point 2. Convective (black line) and radiative (red line) heating of the solid fuel, normalised fuel mass (green line), fuel moisture (blue line), and oxygen (purple line) at (*c*) $x = 270$ m for point 1; and (*d*) $x = 470$ m for point 2.

and gases minus the energy emitted by the fuel at that location. One noticeable difference between the processes at points 1 and 2 is the fact that at point 1, the radiative and convective heat flux peaks are close in magnitude ($\sim$45 kW m^{-2}), whereas the convective heat flux peak ($\sim$30 kW m^{-2}) is significantly larger that the radiative heat flux peak ($\sim$18 kW m^{-2}) at point 2. At point 1, the fact that the convective and radiative peaks occur at the same time indicates the radiative pulse at this point is gaining a large contribution of radiative energy from the hot emitting gases that have engulfed the fuel.

Another feature of these plots is the information that can be obtained from the normalised oxygen concentration curve. The precise magnitude of the normalised oxygen concentration is not the focus of our attention owing to the crude approximations that are made in the combustion model. Rather, the trends shown by the way the oxygen concentration evolves provide important

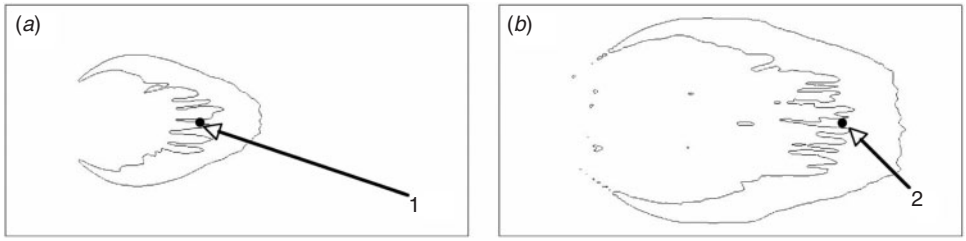

Fig. 7. Fire perimeters at times (*a*) 165 s and (*b*) 285 s depicted by contour lines of solid temperature at 500 K for the GRASSFLAT simulation.

clues about the history and movement of gases in the vicinity of the fire. The onset of the rapid reduction of this value occurs at the same time that the convective heat transfer is starting to rise rapidly and the solid temperature is starting to climb. This is another indication that gases coming from the vicinity of the actively burning cells move to points 1 and 2, which are not burning as strongly at this time. As the gases pass through the upwind burning zone, their oxygen is reduced, and they carry this property to points 1 and 2.

It is interesting to note that the oxygen is already significantly reduced by the time solid fuel falls off quickly. The fact that the oxygen is significantly depleted when the temperature is still relatively low at point 1 and at the same time the convective and radiative heat fluxes are peaking supports the notion that the gases in the cell at that point have come directly from burning locations, and there are very few fresh gases being mixed with the hot radiating gases. This is consistent with the notion that the radiating gas is playing a role in the peak value of the radiative heat flux at that time. The variations in the oxygen concentrations during the period of high temperatures are associated with the intermittent flux of fresher air to the points of interest. The positive fluctuations in the oxygen concentration are directly correlated with the negative pulses in the convective heating and to some degree with the negative fluctuations in the radiative flux. This correlation is due to the fact that fluxes in fresh air over the points will bring cooler gas temperatures (increased convective cooling) and reduced local radiation gaseous sources. The recovery of the oxygen concentration occurs as the fire passes the points and more fresh gases are being entrained from the rear of the fire. Eventually, the local sink of oxygen declines as the reaction rates decline.

Comparison between GRASS, CHAP, and PINE fuels on FLAT topographies

The CHAPFLAT and PINEFLAT simulations show some similarities and some differences in the way the evolving processes interact to produce the simulated fire behaviour. Figs 8 and 9 include plots similar to those in Fig. 6 except they are for the CHAPFLAT and PINEFLAT ground fuel beds (the canopy in PINEFLAT is discussed later). An important note about Fig. 8 is that the time scale for these plots is not the same as those for Figs 6 and 9 because the duration of the burning is much greater in the chaparral fuels than in the other fuel beds. This extended burning period is attributed to the fact that the chaparral fuel bed has a higher bulk density than the other fuel beds (1.25 $kg\,m^{-3}$ for CHAP *v.* 0.46 $kg\,m^{-3}$ for GRASS and ~0.24 $kg\,m^{-3}$ for PINE).

This extended burning period is also reflected in the thickness of the firelines in Fig. 4 when combined with the nominal spread rates of the various simulations. For example, the CHAPFLAT simulation has a heading fireline that is on the order of twice the thickness of the heading GRASSFLAT fireline, and the CHAPFLAT spread rate is on the order of half the GRASSFLAT spread rate. Thus, we might expect that the duration of the CHAPFLAT burning is on the order of four times longer than the GRASSFLAT. A similar comparison can be made with the PINEFLAT, where the heading fireline front is on the order of a third the thickness of the CHAPFLAT and the spread rate is on the order of four thirds the spread rate of CHAPFLAT, so the burning duration of the GRASSFLAT is on the order of one fourth the duration of CHAPFLAT (seen in Fig. 9). In the text below, some noteworthy features of Figs 8 and 9 are mentioned as well as interesting similarities or differences between the various trends with the various fuels. However, many of the ideas discussed for the GRASSFLAT simulations will not be repeated for the other fuel beds even though they apply.

The chaparral simulation has a substantial difference in the burning time between point 1 and point 2, roughly 200 *v.* 80 s. This is attributed to the spatial heterogeneity of the fire front as mentioned in the grass results and shown in Fig. 7. As the fire approaches the point, the resolved wind turbulence increases, but the mean velocity is $<1\,m\,s^{-1}$ owing to the drag of the heavy fuel load. As the temperature starts to climb, there is a negative *u*-velocity similar to that seen in the grass simulations. Then, as the fire passes the points, the *u*-velocities increase to ~4 $m\,s^{-1}$ owing to the reduction in the drag (fuel loads are reduced to 6 and 27% of their original values at points 1 and 2 respectively) and the buoyancy of the fire adds a strong indraft. During the time of high temperatures, the *v*-velocity fluctuations are on the order of 2 $m\,s^{-1}$ but there is very little mean *v*-velocity, whereas the vertical velocity (*w*) in this near-ground layer has a mean velocity of ~1.5 $m\,s^{-1}$ in the early part of this hot time period.

At both chaparral points, the convective heating peaks of ~21 $kW\,m^{-2}$ are at least double the value of the net radiative heat flux peak of ~10 $kW\,m^{-2}$. However, both values are smaller than those seen in the other fuel beds. It is important to remember that a low net radiative heat flux does not mean that there is not energy being absorbed, but rather that the energy absorbed is being balanced by energy being emitted. The reduced values of convective and radiative heating and cooling in the chaparral fuel

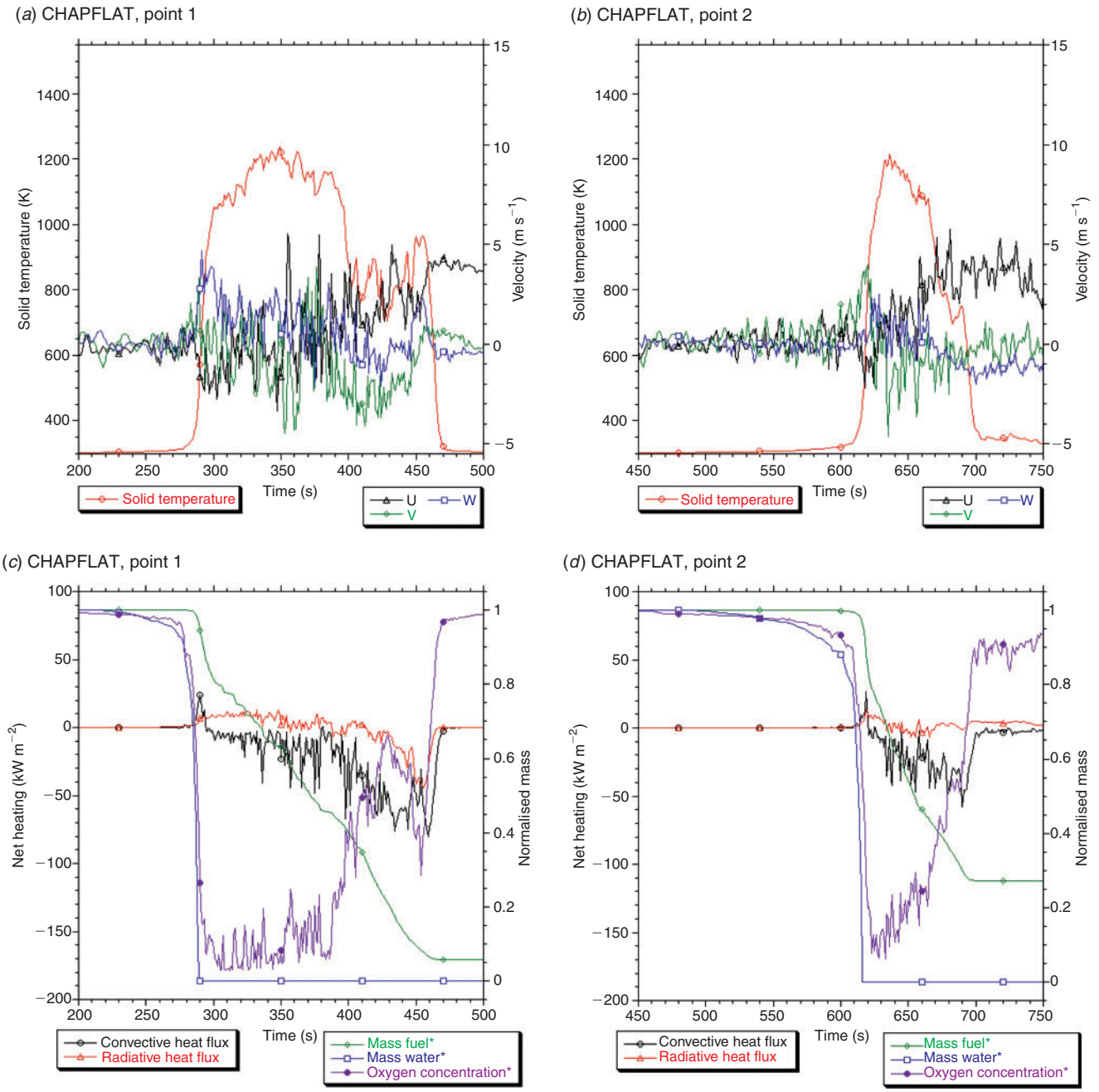

Fig. 8. Time series of quantities from the CHAPFLAT simulation. Solid fuel temperature (red line), u or streamwise (black line), v or crosswind (green line), and w or vertical (blue line) components of the wind velocity at (*a*) $x = 270$ m for point 1; and (*b*) $x = 470$ m for point 2. Convective (black line) and radiative (red line) heating of the solid fuel, normalised fuel mass (green line), fuel moisture (blue line), and oxygen (purple line) at (*c*) $x = 270$ m for point 1; and (*d*) $x = 470$ m for point 2.

beds compared with the other fuel beds are related to the higher fuel loads of the chaparral fuel bed. The larger fuel load and associated larger surface area per unit volume can modify the physics of processes such as changing the air-flow patterns around the fire within the fuel load, reducing the average temperature difference between gas and solids, and causing the radiative heating to not extend as far in front of the fire owing to decreased optical path length. Another factor of the discretisation that occurs is that if the amount of energy being absorbed in two cells is the same, but the amount of remaining fuel in the two cells is different, the average heat flux to the fuel in the cell per unit surface area will be different. These factors also lead to the convective cooling increasing as the fuel gets burned off at both locations. One interesting feature of the evolution of properties at point 1 in the chaparral fire is the decrease in temperature and then small resurgence. The resurgence occurs at the same time as a significant and relatively sustained negative v-velocity (-3 m s^{-1}), an increase in oxygen concentration, and an increase in the fuel loss

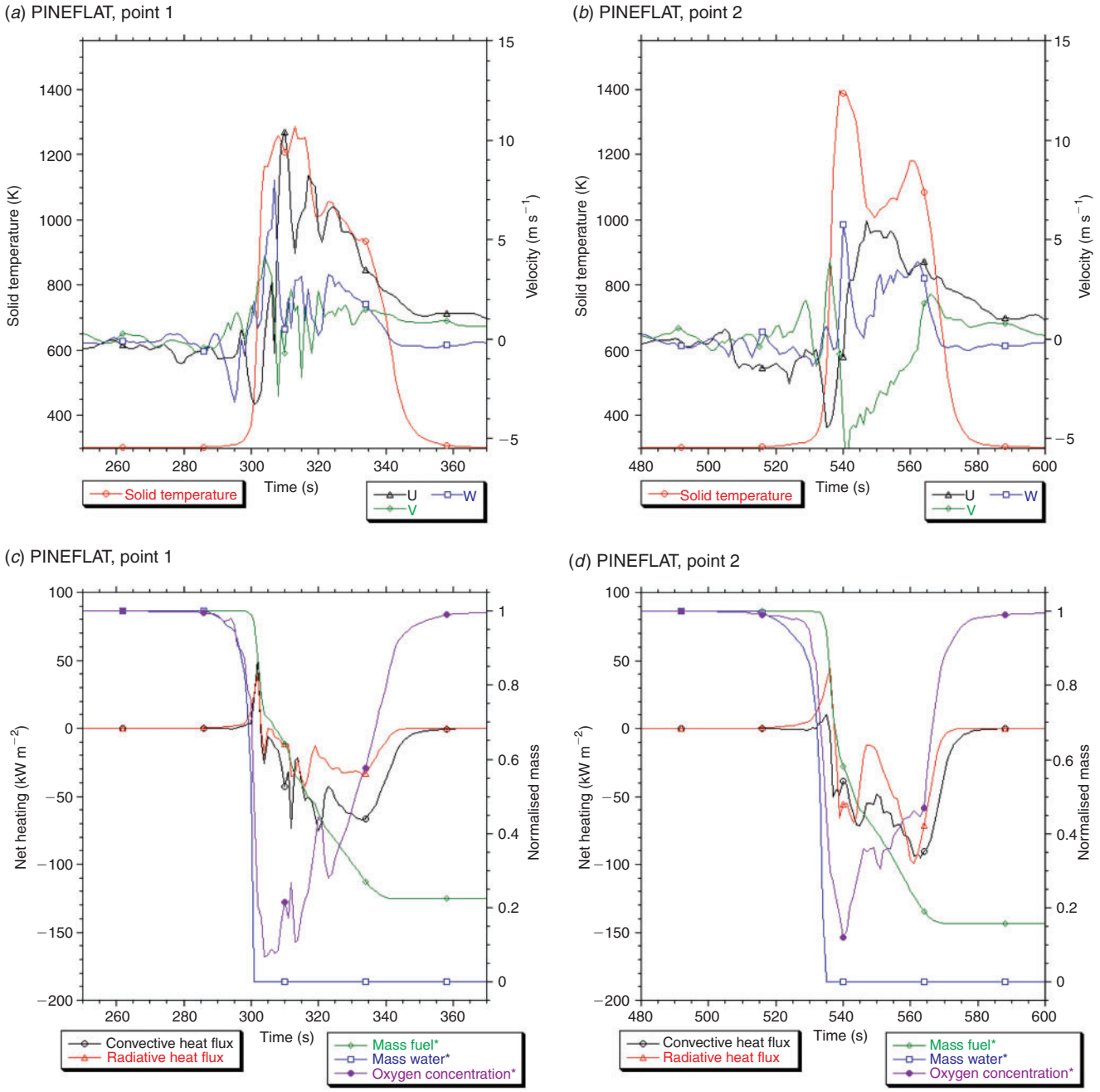

Fig. 9. Time series of quantities from the PINEFLAT simulation. Solid fuel temperature (red line), *u* or streamwise (black line), *v* or crosswind (green line), and *w* or vertical (blue line) components of the wind velocity at (*a*) $x = 270$ m for point 1; and (*b*) $x = 470$ m for point 2. Convective (black line) and radiative (red line) heating of the solid fuel, normalised fuel mass (green line), fuel moisture (blue line), and oxygen (purple line) at (*c*) $x = 270$ m for point 1; and (*d*) $x = 470$ m for point 2.

rate. This seems to be related to a lateral influx of fresh gas that brings in more oxygen to hot fuels and the oxygen-limited fire.

An interesting correlation that can be seen in Figs 6 and 8 is that at the locations where the fireline is very deep compared with the other point in the respective simulation (point 2 in the GRASSFLAT simulations and point 1 in the CHAPFLAT simulations), there is an elevated vertical velocity pulse at the time when the temperature rises quickly (along with the already mentioned reversed *u*-velocity pulse), whereas there is minimal vertical velocity and a significant crosswind *v*-velocity at the locations where the fireline thickness is smaller. This correlation appears to be driven by the nature of the coupling between the fire and the atmosphere in these simulations, and was alluded to in Linn and Cunningham (2005) and Cunningham and Linn (2007). If we imagine a simplified model of the fireline being made of a series of tilted counter-rotating vortices as mentioned in

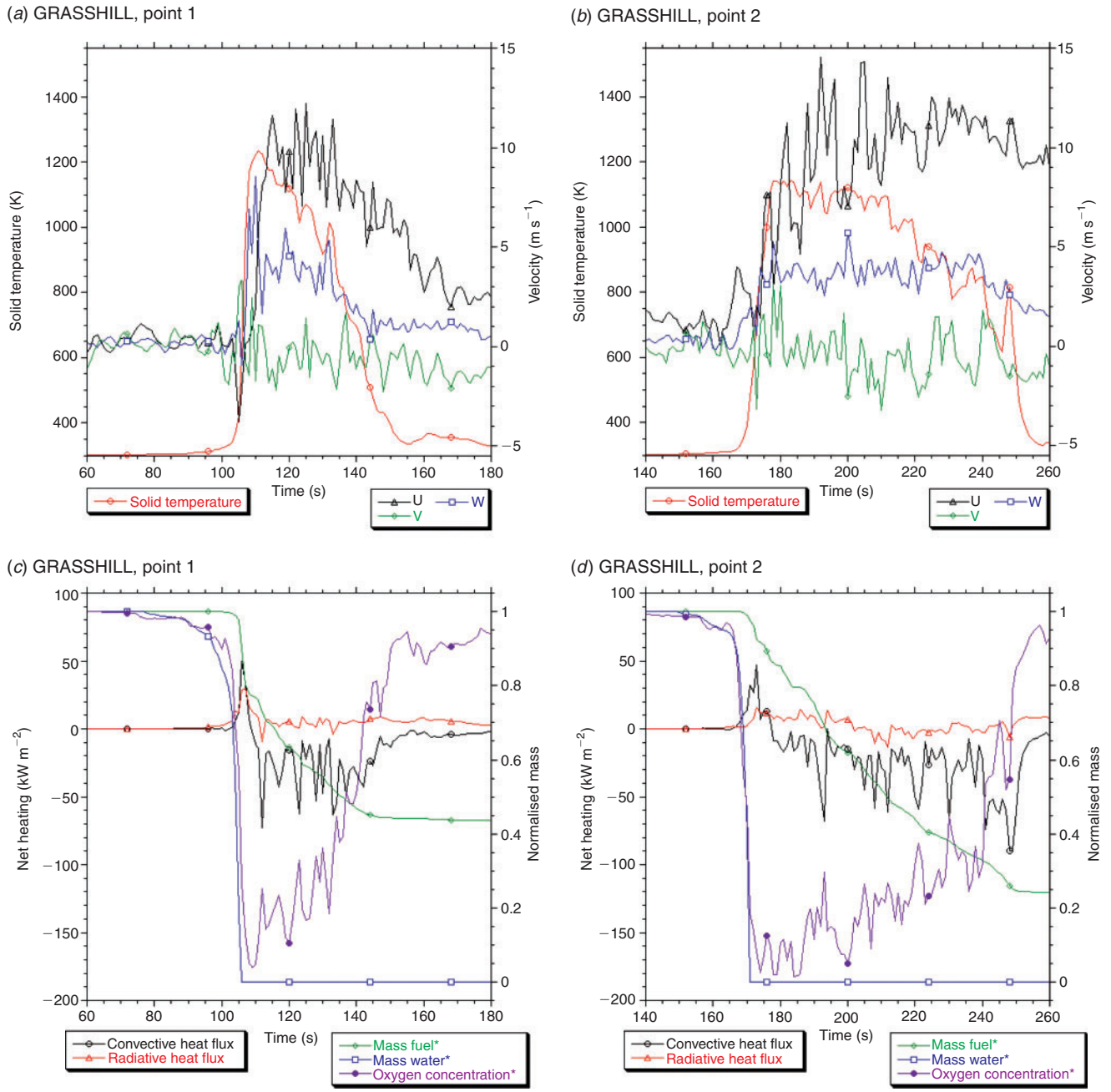

Fig. 10. Time series of quantities from the GRASSHILL simulation. Solid fuel temperature (red line), u or streamwise (black line), v or crosswind (green line), and w or vertical (blue line) components of the wind velocity at (*a*) $x = 270$ m for point 1; and (*b*) $x = 470$ m for point 2. Convective (black line) and radiative (red line) heating of the solid fuel, normalised fuel mass (green line), fuel moisture (blue line), and oxygen (purple line) at (*c*) $x = 270$ m for point 1; and (*d*) $x = 470$ m for point 2.

reference to Fig. 7, the seams where the vortices are converging together have minimal crosswind velocities but significant vertical velocities.

Fig. 9 shows the processes and properties for the ground fuel layer of PINEFLAT at points 1 and 2. Fig. 9*a*, *b* shows an indraft with negative u-velocity before and while the solid temperature starts to rise. The u-velocity increases as the fire moves over points 1 and 2, and then falls off after the fire burns over the point. Before this strong indraft, $-3\,\mathrm{m\,s^{-1}}$ at point 1 and $-4\,\mathrm{m\,s^{-1}}$ at point 2 as seen in Fig. 9*a*, *b*, the velocity is negative ($\sim -1\,\mathrm{m\,s^{-1}}$) for at least 20 s before the fire reaches point 2 and slightly negative for at least 20 s before the fire gets to point 1. This extended period of reversed flow, which is also seen in the grass simulations, is indicative of the larger-scale recirculations that exist in front of the fire when the drag of the fuel is not able to damp out these velocities. The duration of the fire at both point 1

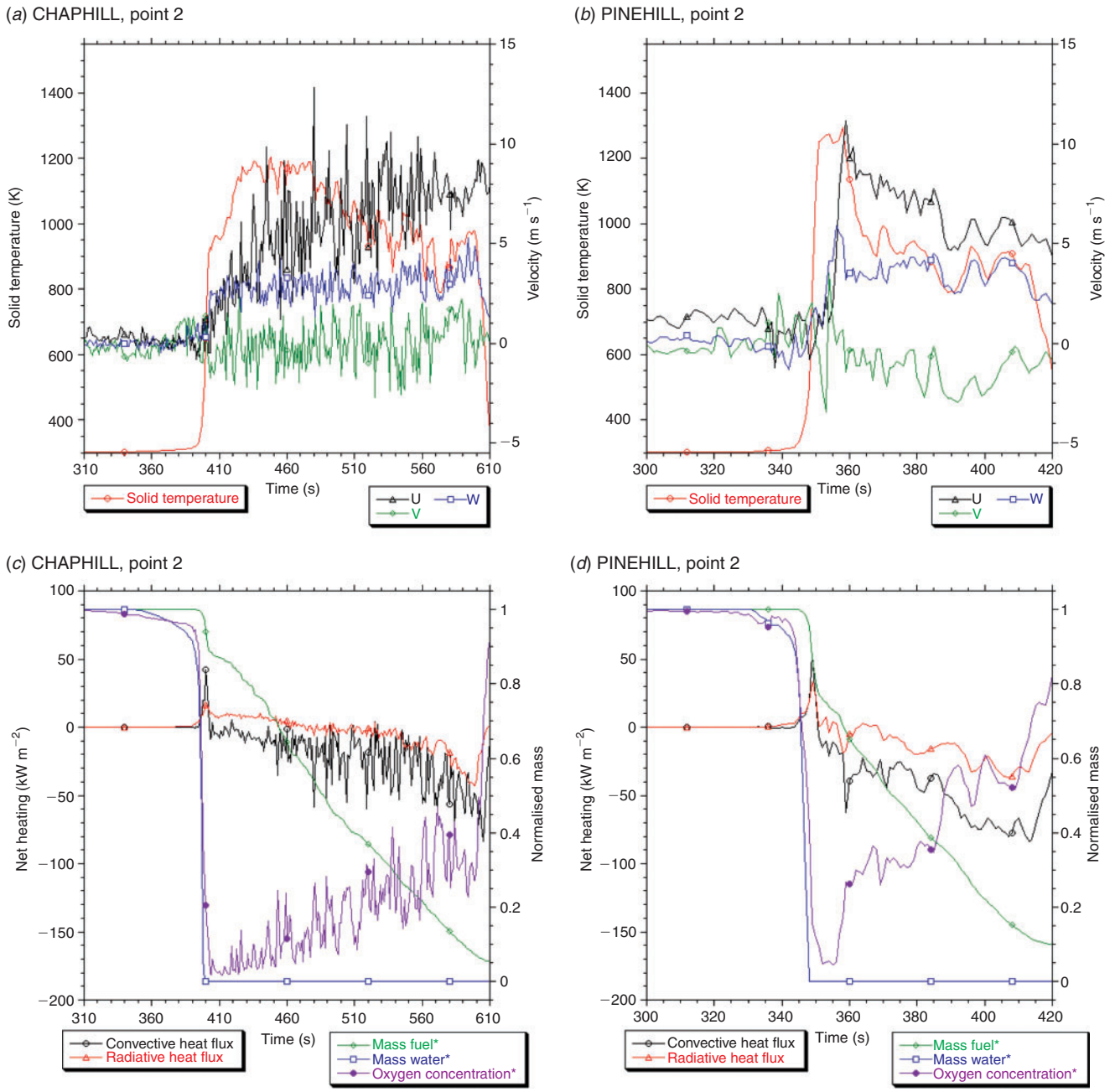

Fig. 11. Time series of quantities from the CHAPHILL and PINEHILL simulations at $x = 470$ m. Solid fuel temperature (red line), u or streamwise (black line), v or crosswind (green line), and w or vertical (blue line) components of the wind velocity for (*a*) CHAPHILL point 2; and (*b*) PINEHILL point 2. Convective (black line) and radiative (red line) heating of the solid fuel, normalised fuel mass (green line), fuel moisture (blue line), and oxygen (purple line) for (*c*) CHAPHILL point 2; and (*d*) PINEHILL point 2.

and point 2 in PINEFLAT is ~40 s. The similarity of these times is related to the fact that the fireline in the litter and grass layer under the pine canopy does not have as much heterogeneity in the thickness of the fireline as seen in Fig. 4*e*. The duration of the burning period of the ground fuel in the PINEFLAT simulation and the relatively thin fireline seen in Fig. 4*e* as compared with Fig. 4*a*, *c* is caused by the fact that there is a much smaller amount of fuel to burn.

The understorey of the PINEFLAT fuel bed experiences preheating and drying at points 1 and 2 over periods of 10 and 20 s respectively and responding convective cooling. One notable difference between point 2 in the PINEFLAT simulation and the other ground-level points in the three FLAT simulations is that the peak radiative heating is much larger in magnitude at this location than the convective heating peak. This issue warrants more investigation in order to better understand

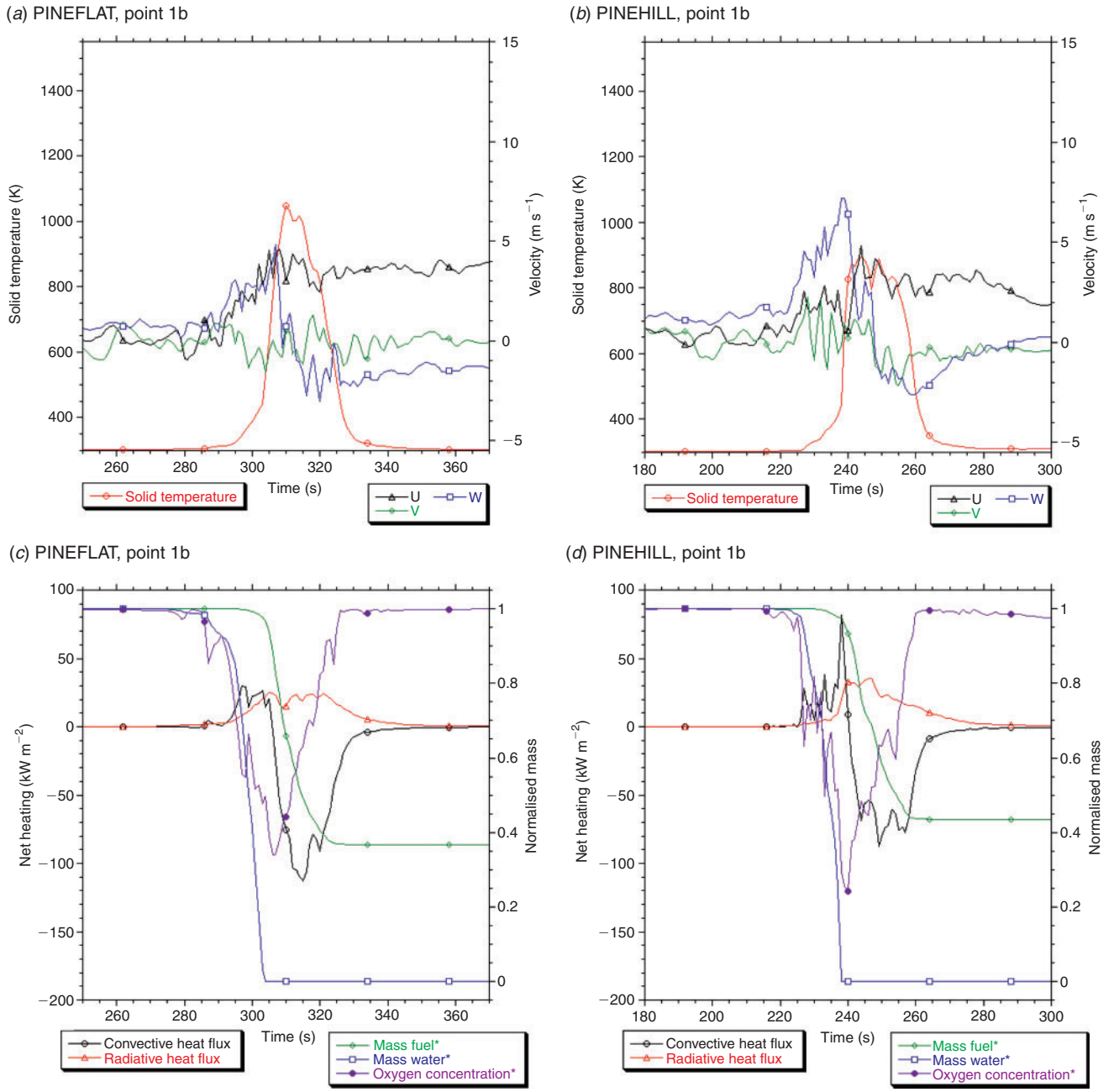

Fig. 12. Time series of quantities from the PINEFLAT and PINEHILL simulations at $x = 270$ m and $z = 11$ m (mid-canopy). Solid fuel temperature (red line), u or streamwise (black line), v or crosswind (green line), and w or vertical (blue line) components of the wind velocity for (*a*) PINEFLAT point 1b; and (*b*) PINEHILL point 1b. Convective (black line) and radiative (red line) heating of the solid fuel, normalised fuel mass (green line), fuel moisture (blue line), and oxygen (purple line) for (*c*) PINEFLAT point 1b; and (*d*) PINEHILL point 1b.

the situations that lead to this change in balance of heat-transfer processes; however, the fact that the convective and radiative heat peak at nearly the same time indicates that hot radiating gases have engulfed the fuels. The fuels have already heated up above 800 K by this time. The higher fuel temperatures significantly reduce the convective heating potential, but the temperature is not high enough for the solid radiative emissions to balance the absorbed radiation. This is likely to be a function of a circumstantial correlation between the various intermittent processes and the inhomogeneous fuels, but it is also likely that this is affected by the more vertically distributed nature of the pine fuels.

There is a strong lateral indraft of air being drawn over point 2 by a neighbouring cell (shown by the 3.7-m s^{-1} v-velocity in Fig. 9*b*) that reduces the gas temperature and thus reduces the magnitude of the convective heating pulse. At point 1 in PINEFLAT, there is no strong lateral flow being induced by a neighbouring cell, so the vertical velocity begins to rise ~1 s after the

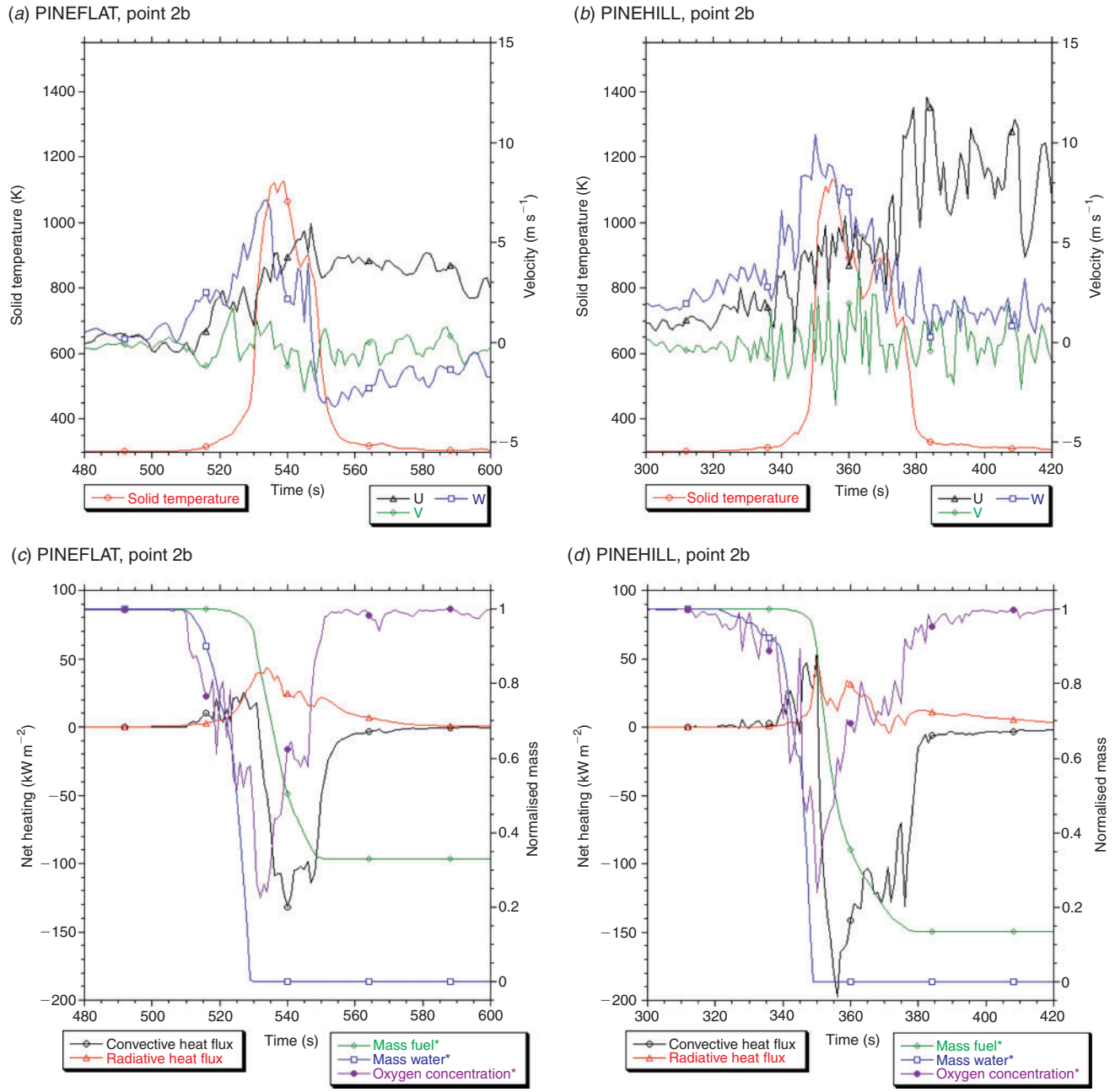

Fig. 13. Time series of quantities from the PINEFLAT and PINEHILL simulations at $x = 470$ m and $z = 11$ m (mid-canopy). Solid fuel temperature (red line), u or streamwise (black line), v or crosswind (green line), and w or vertical (blue line) components of the wind velocity for (*a*) PINEFLAT point 2b; and (*b*) PINEHILL point 2b. Convective (black line) and radiative (red line) heating of the solid fuel, normalised fuel mass (green line), fuel moisture (blue line), and oxygen (purple line) for (*c*) PINEFLAT point 2b; and (*d*) PINEHILL point 2b.

temperature rises quickly. Another indication that there is a difference in the flow pattern at PINEFLAT point 2 compared with most of the other points is the fact that the vertical velocity is very small until ~4 s after active burning begins. Also, the large positive u-velocity that occurs ~6 s after the active burning begins is indicative of hot gases from farther back in the fireline being driven towards point 2 and contributing to its convective heating. At point 1 in PINEFLAT, this effect is much less significant.

Another difference between the PINEFLAT points and the GRASSFLAT or CHAPFLAT points is the structure of the solid temperature profile. In PINEFLAT, the temperature peaks and then declines quickly, whereas in the other fuel beds, the temperature stays near its peak for longer periods of time. The more rapid decline in the solid temperature after only 10 to 15 s is associated with the stronger radiative cooling that is present in PINEFLAT than in the other fuel beds. This stronger radiative

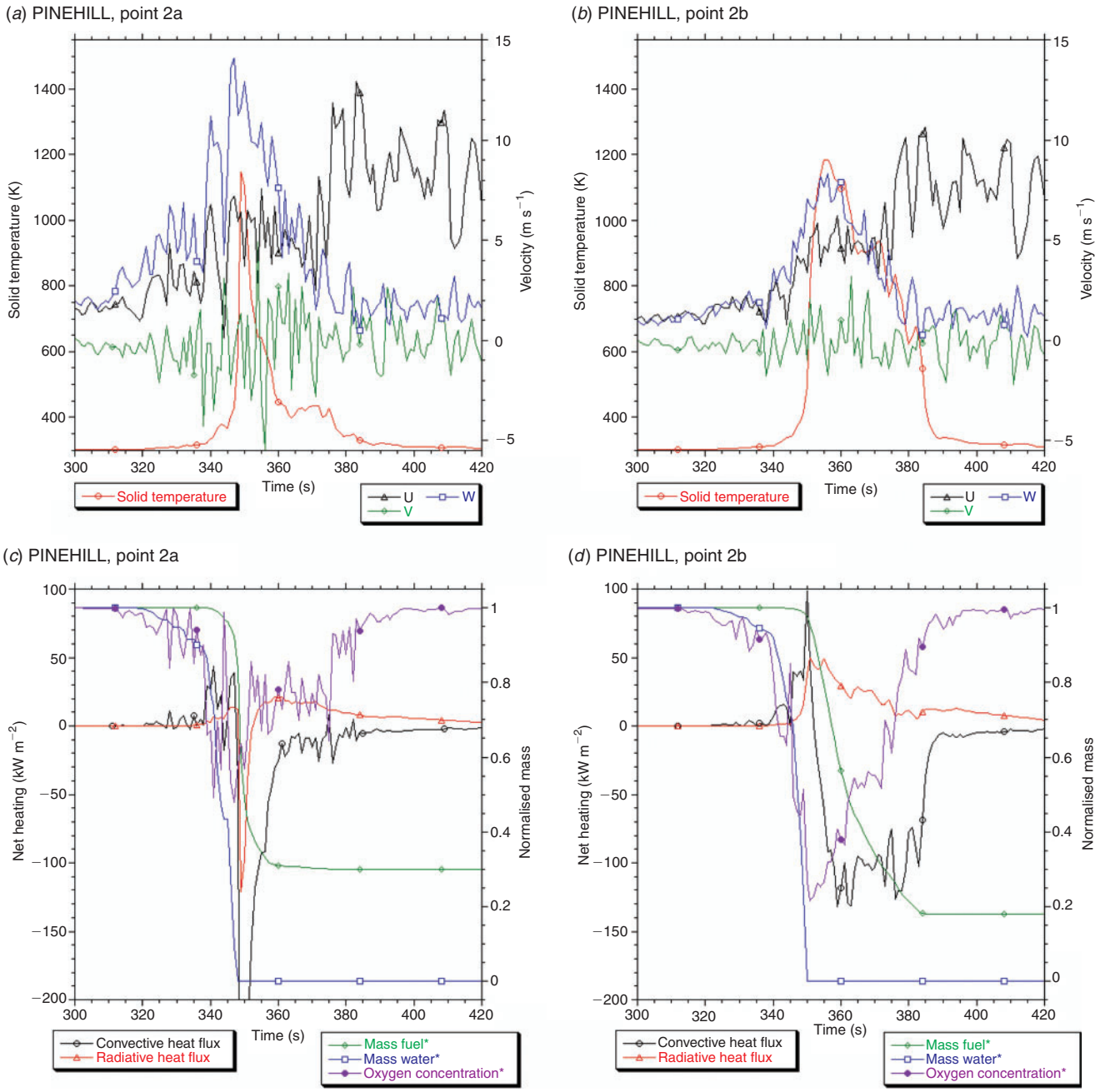

Fig. 14. Time series of quantities from the PINEHILL simulation at $x = 468$ m (point 2a) or $x = 472$ m (point 2c) and $z = 11$ m (mid-canopy). Solid fuel temperature (red line), u or streamwise (black line), v or crosswind (green line), and w or vertical (blue line) components of the wind velocity for (*a*) PINEHILL point 2a; and (*b*) PINEHILL point 2b. Convective (black line) and radiative (red line) heating of the solid fuel, normalised fuel mass (green line), fuel moisture (blue line), and oxygen (purple line) for (*c*) PINEHILL point 2a; and (*d*) PINEHILL point 2b.

cooling happens when the temperatures are very high and the amount of surrounding material radiating towards the points drops off quickly owing to changes in gas composition and the fact that the ground and crown fires have moved forward and are leaning away from the points of interest. The wind velocities in the vicinity of the ground points in PINEFLAT are also higher in magnitude than the points in the other fuel beds. This causes larger intermittent convective cooling periods that help bring down the temperature. Another effect of these larger intermittent velocities, which can be seen in the large negative v-velocity in Fig. 9*b* for point 2 and the very large gusty u-velocities in Fig. 9*a* for point 1, is the fact that they carry in fresh air that supplies oxygen, as illustrated in Fig. 9*c*, *d*, to the fires and allows them to resurge.

In all three fuel beds, as the fire moves past the point, the u-velocity increases and the w-velocity becomes negative. These

negative values are indicative of the indraft at the bottom of the fire.

Ground fire behaviour for GRASS fuel on HILL topography

Fig. 10 illustrates the evolution in processes for points 1 and 2 in the GRASSHILL simulation. As discussed above, because points 1 and 2 are equally distant from the centre of the hill, the local slope of 0.366 (an angle of 20° above horizontal) at the respective locations on the hill is the same at points 1 and 2.

Fig. 10 is included in order to highlight some of the differences in the simulated combination of physical processes that are caused by differences in slope. In Fig. 10*a*, *b*, the most obvious differences between the behaviour in GRASSHILL at points 1 and 2 and those in Fig. 6*a*, *b* for GRASSFLAT are the evolution of the *u*- and *w*-velocities and the shape of the solid temperature profile. There are essentially no negative *u*-velocities before the fire reaches points 1 and 2 in the GRASSHILL simulation, whereas in the GRASSFLAT simulation, there are negative *u*-velocities, indicating intermittent reversed flows in front of the fire connected with the entrainment in front of the fire. The absence of the reversed entrainment velocities in the GRASSHILL simulation indicates that the buoyant plume is closer to the ground in this simulation and the entrainment is constricted on this side. The fact that the entrainment on the upslope side of the fire is constricted forces the entrainment on the other sides of the fire to be stronger. This then pushes the rising gases closer to the ground and enhances the preheating of the unburned fuel, which helps to accelerate the fire. The *u*-velocities in the GRASSHILL simulation climb very rapidly to nearly $10\,m\,s^{-1}$ as the temperature rises rapidly, whereas these velocities only rise to values of $\sim 5\,m\,s^{-1}$ by the end of the intense burning period on the flat ground. At point 1 (near the bottom of the hill) and point 2 (near the top of the hill) in GRASSHILL, the velocities intermittently reach values of 12 and $14\,m\,s^{-1}$ respectively during the intense burning time and then fall off to 6 and $10\,m\,s^{-1}$ by the time the temperatures have dropped below 400 K. This trend towards higher *u*-velocities is partially due to the fact that the buoyancy-induced indraft is trying to draw air from a position that is more exposed to the ambient wind when the fuel bed is on a slope. In addition, winds impinging on the hillside create an elevated pressure that feeds the buoyancy-induced indraft and contribute to the effect. At the same time, the plume entrains itself closer to the ground and there is a larger *u* component to the indraft. The fact that the plume is closer to the hill affects the recirculation on the upslope side of the fire, and at point 2 in the GRASSHILL simulation, the reversal of flow in front of the fire does not exist.

An effect of the elevated wind speeds is the erosion of the solid temperatures over time, whereas in the GRASSFLAT simulation, the solid temperature stays high until the burning is essentially done. The rapid reduction in temperature at point 1 leads to less complete burning than at the ground fuel points in the FLAT simulations. The vertical winds at both points in the GRASSHILL simulation are higher during the intense burning period than in the GRASSFLAT simulation, and these stronger vertical winds could also be fed by the impingement of the wind on the slope.

In Fig. 10*c*, *d*, the convective heating peaks at both points ($\sim 50\,kW\,m^{-2}$) is substantially higher than the radiative heating peaks (~ 30 and $10\,kW\,m^{-2}$ at points 1 and 2 respectively), and the convective cooling at both points is of the same order of magnitude as at point 1 in the GRASSFLAT simulation ($\sim -50\,kW\,m^{-2}$). The net radiative heating and cooling magnitudes at the points in the GRASSHILL simulation are much less than in the GRASSFLAT simulation, partially because in the later stages of burning (where the GRASSFLAT radiative cooling was most significant), the temperatures in GRASSHILL are significantly reduced.

Ground fire behaviour for PINE and CHAP fuels on HILL topography

Fig. 11 includes plots for point 2 in the CHAPHILL and PINEHILL simulations. The most significant difference between the behaviour of processes and properties at point 2 in the CHAPFLAT and CHAPHILL simulations is that, as seen in the grass fires, the *u*-velocities are much stronger in the burning region in the CHAPHILL simulation, $\sim 8\,m\,s^{-1}$ with $\pm 3\,m\,s^{-1}$ fluctuations, as opposed to $\sim 3\,m\,s^{-1}$ with $\pm 2\,m\,s^{-1}$ fluctuations for CHAPFLAT. This may be due to the winds impinging on the hill, and the fact that the wind encounters fewer obstructions to reach the points because the slope effectively elevates the fuel at both points 1 and 2 above the fuel just downslope (upwind) of them.

Fig. 11*b*, *d* illustrates the *u*-velocity patterns in the PINEHILL simulation, which show elevated values, sustained above $7\,m\,s^{-1}$ and reaching as high as $11\,m\,s^{-1}$, during the most intense burning and after the temperatures drop. There is also no reversed *u*-velocity in front of the fire as seen in the GRASSHILL simulation at point 2. In the PINEHILL simulation at point 2, there is not a significant lateral indraft, so the oxygen concentration recovery that happened at point 2 on PINEFLAT does not occur to as great an extent. Also, the solid temperatures do not recover to a second peak value. Another effect that occurs in the GRASSHILL, CHAPHILL, and PINEHILL simulations at point 2 is the radiative cooling is reduced. There is not a substantial increase in the convective cooling, even though the winds are much larger, because hot gases continue to be funnelled to these points from the flanking portion of the fire owing to the more pointed shape (described in detail in Linn *et al*. 2007). This effect results in longer burning periods.

Comparison of canopy fires

Canopy fire behaviour at point 1b for FLAT and HILL topographies

The same two points (*x* and *y* location) and methodology can be used to compare the coupling between processes in the canopy of PINEFLAT and PINEHILL. This is similar to the work described in Linn *et al*. (2005), except in the present case, both locations have the same local tree arrangement. Thus, the only focus of our examination will be the impact of slope and position on the slope on fire behaviour. We first examine the effect of slope on the canopy fires at point 1 by comparing the evolution of properties and processes shown in Fig. 12, which depicts the evolution of properties 11 m above the ground (point 1b) for PINEFLAT and PINEHILL.

This figure illustrates some significant differences between the trends seen in Figs 6 and 8–11 for the ground fuels. At point

1b in PINEFLAT and PINEHILL, the peak temperature for the canopy fuels is ~200 K lower than at point 1. Also, the duration of the high temperature is only ~30 s at point 1b in the PINEFLAT and PINEHILL simulations. This duration is connected to the thickness of the firelines in Fig. 4*e*, *f*, which are thinner than those of the GRASS and CHAP simulations. In this case, the duration of the burning is affected by the canopy fuel load, which is not as high as the CHAP fuel load, and the extra ventilation available to the canopy fuels because they are elevated. This is further illustrated by the fact that the minimum oxygen concentration is higher than it is in the ground fuel beds. In both of these simulations, the peak *u*-velocity is ~4 m s^{-1}. There is no time during the simulation where the *u*-velocity is significantly negative, indicating no major recirculations at the canopy level in the PINEFLAT or PINEHILL simulation. In fact, for both the PINEFLAT and PINEHILL simulations, the *u*-velocity has already risen more than 2 m s^{-1} above its prefire value by the time the solid temperature begins to rise quickly. Another substantial difference from the ground fuels can be seen in the evolution of the *w*-velocity. In the ground fuel plots, the vertical velocities did not rise until the solid temperature was rising quickly. Fig. 12*a*, *b* shows that the vertical velocity has nearly peaked in the canopy fuel at point 1b for both the PINEFLAT and PINEHILL simulations at the onset of the active burning. This is due to the fact that the heat from the ground fuels is being carried upward at a forward-leaning angle. The depletion of oxygen long before the fuels start to burn is another indication that plume gases reaching the canopy points before the active burning begins are coming from fires lower in the fuel stratum. In fact, the ignition of the canopy and ground fuels at point 1 in PINEFLAT occur at approximately the same time, but the vertical updraft carrying heated gases begins almost 10 s before. At point 1b, we can approximate the vertical velocity 10 s before active burning as 2 m s^{-1} for PINEFLAT and 5 m s^{-1} for PINEHILL, and the *u*-velocity as 2 m s^{-1} for both simulations. Thus, we can approximate the plume angle at point 1b as ~45° for PINEFLAT and 70° above horizontal for PINEHILL. At this point in the canopy simulations, as the temperature peaks, the vertical velocity starts to drop. This indicates that much of the driving force for the vertical velocity is provided by fuels below and not the temperature of the fuel at this location itself. In the canopy fuels, the vertical velocity becomes negative before the temperature cools off significantly, which is indicative of the strong indraft to the lower portion of the canopy fires and the ground fires.

The convective heat flux to the fuels shows a direct response to the gases rising from below by having pulses of high convective heat flux beginning more than 7 s before the active burning begins. The early convective heating pulses are stronger at point 1b in PINEHILL than point 1b in PINEFLAT, but even on the flat terrain they exist. In the PINEHILL simulation, the convective heating peak is more than 80 kW m^{-2}, and then becomes negative at almost the same magnitude. In the PINEFLAT simulation, the convective cooling flux reaches more than 100 kW m^{-2}. The sustained strong convective cooling is due to the previously mentioned downdraft of fresh air that is being pulled to lower positions in the canopy and the ground fire. At point 1b in PINEFLAT and PINEHILL, the convective cooling helps to quench the fires before all of the mass is consumed, leaving ~37 and 44% of the solid fuel mass intact after the fire has passed. The net radiative fluxes to point 1b in these simulations are positive throughout the passing of the fire. This result is somewhat counter-intuitive and warrants further investigation; however, in the interpretation of this result, it is important to realise that the quantity being plotted is the absorbed energy minus the released energy. This quantity can be positive if we consider a location where the convective cooling has kept the temperature low compared with much of its surroundings. Thus, the radiated flux from that particular location is lower than the energy received from surrounding radiative sources such as the fuels on the ground, which are at a much higher temperature. In these simulations, the effect appears to be due to the fact that there are hotter gases and solids around point 1b including the ground fuels. Even though the current radiation scheme has worked fairly well for many wildfire situations, investigations with more computationally expensive radiation transport methods such as Monte Carlo are being used in order to determine if this effect is an artefact of the current radiation model.

Canopy fire behaviour at point 2b for FLAT and HILL topographies

Because the local fuel structure at point 2b is the same as the local fuel structure at point 1b, we can compare the behaviour at these two points and gain some feeling for the effects of the evolution of the fire on flat ground and on terrain. Fig. 13 provides information for point 2b similar to that provided in Fig. 12 for point 1b. The plots in Fig. 13*a*, *c* illustrate that the behaviour at point 2b is very similar to the behaviour at point 1b for the PINEFLAT simulation with only a few small differences. The peak vertical velocity at point 2b, ~7 m s^{-1}, is larger than that seen at point 1b and the horizontal velocity at point 2b peaks later with respect to the active burning period than at point 1b. The convective heating pulses start earlier at point 2b, and the peak radiative heating flux is larger than the net peak convective heating flux at point 2b. Otherwise, most of the trends are the same at points 1b and 2b, including the reduced consumption of the fuel.

Fig. 13*b*, *d* illustrates the evolution of properties at point 2b in PINEHILL. The differences between PINEHILL points 1b and 2b are much greater than those for PINEFLAT points 1b and 2b. At point 2b, the temperature reaches a value of more that 1130 K and the duration of the high temperatures is ~35 s, whereas at point 1b, the temperature peaks at close to 900 K and the duration of the fire is closer to 22 s. The vertical and horizontal velocities begin rising at least 30 s before the active burning, and the peak values are much larger at 10 and 12 m s^{-1} respectively. The large *u*-velocity has a mean value of ~9 m s^{-1} that occurs after the solid temperature has dropped below 400 K. There are ±3 m s^{-1} fluctuations in this indraft. This is comparable with the large *u*-velocity values that occur at point 1b in PINEHILL early in the active burning and have a mean value ~3 m s^{-1} with ±1 m s^{-1} fluctuations. At point 2b, the vertical velocity never goes negative, and is ~1.8 m s^{-1} upward before the fire reaches the point and 1.8 m s^{-1} after. The strong indraft pulled in behind the fire at PINEHILL point 2b is coming up the slope, not pulled down from above.

Fig. 13*d* illustrates the effects of the extended period of hot gases rising from below (mentioned above) through the

much longer duration of the convective heating pulses before the active burning and the earlier signs of oxygen depletion in PINEHILL point 2b. The larger *u*- and *w*-velocities cause a much bigger convective cooling peak, $-195\,\mathrm{kW\,m^{-2}}$, when the temperature reaches its peak. This convective cooling brings the temperature back down. The radiative heating at point 2b of PINEHILL is much more variable than at point 1b owing to the larger fluctuations in the solid temperature and the variations in the wind field that brings radiating gases near the point. The differences between the PINEHILL point 2b and the PINEFLAT point 2b have numerous similarities to those between the PINEHILL point 2b and point 1b discussed above.

Local heterogeneity

In PINEFLAT and PINEHILL, the Ponderosa canopy has considerable inhomogeneity, as seen in Fig. 2. Therefore, it is important to realise (as suggested in Linn *et al*. 2005) that the interactions between processes at a single point are not representative of all points in the simulated fuel bed, even at the same height. This is analogous to saying that if measurements in the field are taken at different locations with respect to a clump of trees (i.e. leading edge of the clump, deep within the clump), the winds, solid temperature evolution, and heat transfer could be very different. This is further complicated by the fact that the location of one clump of trees with respect to another changes the processes at a single location. The temporal sequence of wind gusts and bursts with respect to the time when the fire reaches a clump of trees may also play a role in the way a clump of trees burns. In order to gain a perspective on the evolution of the processes that combine to produce the simulated fire behaviour in the PINE fuel bed at different locations and with different slopes, two additional locations centred around point 2b ($x = 470$ m) are studied. Point 2a is located downwind from point 2b at $x = 468$ m, and point 2c is upwind from point 2b at $x = 472$ m. Fig. 14 contains plots for points 2a and 2c for PINEHILL.

These plots can be combined with Fig. 13*b*, *d* to give a sense of how much the fire behaviour varies across a patch of trees. Point 2a is near the leading edge of a patch of trees with neighbouring point 2b in the middle of the patch and point 2c closer to the back. By looking at Figs 14*a*, 13*b*, and 14*b*, we can see that being on the leading edge of the patch of trees exposes point 2a to winds that have had less drag and less heat exchange than the other two locations. At point 2a, the oxygen concentrations, temperature profiles, water loss, and convective heating spikes that start as much as 35 s before the active burning are correlated with *u*- and *w*-winds that reach point 2a without being slowed or preheated as much as for the other points. These velocities have mean values of $\sim$2 and 4 $\mathrm{m\,s^{-1}}$, with fluctuations of $\sim$2.5 $\mathrm{m\,s^{-1}}$ near the time when the active burning starts. The *v*-velocity also shows strong fluctuations in this period, which is indicative of the three-dimensional structure of the turbulent indrafts that are consistent with the fluctuations in the oxygen concentration and convective heating at this time. The winds and gusts at point 2b are damped by the drag of upwind fuels at and below point 2a. This is even more apparent at point 2c. The peak values of the vertical velocities at points 2a, 2b, and 2c are 14, 10, and 9 $\mathrm{m\,s^{-1}}$ respectively during the active burning, but they all fall off to $\sim$2 $\mathrm{m\,s^{-1}}$ after the fire passes. After the fire has depleted some of the mass at these locations, the fluctuations and magnitudes of the velocities are much more similar, as can be seen by comparing the values at the right side of Figs 14*a*, 13*b*, and 14*b*.

At point 2a, the solid temperature and mass loss are quite different from those at points 2b and 2c, because the high-temperature region, above 700 K, only lasts for $\sim$5 s, and 15 s above 400 K. The rapid fall of the temperature coincides with a time when there is strong convective cooling of $-250\,\mathrm{kW\,m^{-2}}$ compared with peak values of -200 and $-130\,\mathrm{kW\,m^{-2}}$ at points 2b and 2c. In addition, there is a very strong radiative cooling flux of $-110\,\mathrm{kW\,m^{-2}}$ at this time, indicating that there is a lot of energy being lost radiatively and very little radiative energy being absorbed. This is partially due to the fact that the gas passing through the cell has a lot of fresh air and is at a lower temperature than that available to the cells farther back in the patch of trees. The gases in the cell therefore do not radiate as much energy to point 2a. This issue is under further investigation. As soon as the temperature falls off at point 2a, the radiation flux becomes positive again and the convective cooling declines in magnitude, allowing the temperature to stay at $\sim$400 K for $\sim$10 more seconds. The quick extinction of the fuel at this point leaves $\sim$30% of the fuel unburned. This can be compared with points 2b and 2c, where there is minimal radiative cooling and over 80% of the mass is consumed. Another effect of the heterogeneity of the fire and fuel is that the oxygen depletion becomes more significant from point 2a to 2b and then to 2c. This building effect is natural as point 2c is receiving gasses that have come through a burning patch of trees, whereas point 2a has greater access to fresh gases. Related to this notion is the fact that the maximum convective heating spike increases and the convective cooling decreases from point 2a to 2b, and then to 2c. This is because the gases have a greater chance to absorb heat as they travel to the points deeper in the patch. Many of these effects of position within a patch of crown fuels have been seen in laboratory experiments performed by Tachajapong *et al*. (2006). In these laboratory experiments, the leading edge of a patch of crown fuels behaved very differently than the fuels deeper in the patch.

Conclusions

Six simulations were used to examine some of the independent and coupled effects of fuel structure and upslope topography on simulated fire behaviour generated by a physics-based wildfire model, FIRETEC. Landscape-scale indicators such as fire shape and downwind fire spread were examined as well as 2 m-scale averaged values for processes and properties that govern the larger-scale aspects of fire behaviour. This examination of these six simulations can only serve as a sample of some of the effects. It is currently difficult to validate the process-level information; however, many of the macroscopic trends seen in these simulations and other FIRETEC applications agree well with observed behaviours. Thus, the results of the analyses performed here can be used as topics for future research, and will hopefully be valuable for those designing field experiments in the future. One of these macroscopic trends that have been observed and are evident in the simulations is the acceleration of fires when they spread uphill. This is shown in these simulations by the overall fire behaviour, and some of the mechanisms causing the behaviour, such as reduced upslope entrainment and stronger

winds from behind the fire front, are illustrated at specific locations. The difference in the pointed shape of the heading fire on a slope from the more rounded heading fire shape on flat topography is evident in these simulations. The simulations also show the strong dependence of fireline thickness on fuel bed characteristics, as illustrated by the ponderosa pine simulations having a much narrower fireline than the grass or chaparral firelines.

In these simulations, fuel bed characteristics (load, structure, heterogeneity, and moisture) have a significant effect on the spread rate and perimeter shape of the fires on both flat ground and on an idealised smooth hill topography. The fires in chaparral fuel beds have more lateral spread and spread downwind more slowly than those in the ponderosa pine fuel bed, which have minimal lateral spread. The grass fires have the most lateral spread and travel the fastest. The differences between these spread patterns on flat ground is largely due to the fuel load, because the more heat is produced, the more the fire's buoyant plume can block the ambient wind. Also, the distribution of the fuels is important because the ability of the wind to penetrate the fuel bed and convectively move heat from one location to another is an important factor. It should also be noted that the moistures in the various simulated fuel beds are different because they are designed to represent what is found in nature, and these differences in moisture can contribute to the variations in fire behaviour.

The slope also has a significant effect on the spread rate and spread pattern. In each simulation, the spread rate is faster and the head fire shape is more pointed on the upslope topography than on the flat ground. A more interesting result of these simulations is the fact that the slope induces different acceleration and deceleration patterns in the various fuel beds. The chaparral and grass fuel fires had more gradual accelerations than the fire in the pine fuel bed. Another trend seen in these simulations is that the local slope of the hill and a single nominal wind speed would not have been adequate to predict the spread rates. All of the upslope simulations showed that the spread rate is not the same at a point near the bottom of the hill and a point near the top of the hill, even though they have the same slope.

For the simulations on flat ground, several observations can be made from looking at the data from specific locations near the centreline of the fire. Care was taken to try to remove the effects of local vegetation heterogeneities, and therefore the fact that some of the processes and properties are different at similar locations implies that they evolve with time or are heterogeneous in space. The possible significance of the evolution or heterogeneity of the properties or processes deserves considerable thought when taking measurements in the field. A single point measurement might not be representative of the average behaviour, and the fluctuations might be equally important.

The simulations on the upslope topography show some similarities to those on the flat ground, but there are also some differences in the processes and properties when we look at specific locations near the bottom and near the top of the hill that have the same slope. There are differences in the wind movement around the fire on both the upwind and downwind (downslope and upslope) side of the fire. These differences in air movement change some of the influences of convective and radiative heat transfer. The influence of the slope is different for the processes in fires with different fuel structures. The influences of the slope are also different at different locations on the hill, even if the local slope is the same. The effects of the hill seem to grow as the fire moves up the hill, especially in the grass and pine fuel beds. The chaparral fuel bed seems to have less of a building or cumulative effect as the fire moves up the slope, probably owing to the larger amount of drag and greater amount of heat being released.

The overstorey of the pine fuel bed has different behaviours than the understorey of that fuel bed or the other fuel beds tested. This is largely due to the added ventilation from the sides and below that the canopy fuels are subject to. As expected, the canopy fire behaviour seems to be strongly affected by the hot plume coming from lower fires in the fuel stratum. The canopy fires are also strongly affected by the slope. The indraft to the canopy can be more easily aligned with the rising plume because a significant fraction of the indraft originates below the canopy. The canopy fires do not have the recirculations with negative streamwise velocities that occur in the fire's ground fuel beds, which is also owing to the added ventilation to the canopy.

The specific location of the points chosen to look at the canopy processes appears to be quite important. This effect is illustrated by the fact that three consecutive locations in the canopy, spanning a single patch of trees, show a very different set of process balances and magnitudes. It is important for future research to better understand how to account for the heterogeneity of the fuel and the winds around the fuel without having to capture all of the details. An important question is what level of detail is critical and how can we represent the unresolved details if we are unable to model them or to collect wind or vegetation data to describe them. This will be a topic for future research.

This method of looking at the individual processes that govern fire behaviour at specific locations is a valuable approach to study the interaction between the processes and their local impact on fire behaviour, but this particular study has its limitations. Two locations do not provide an adequate sample to be able to draw solid conclusions about the evolution of the details of process interactions as they move up a slope because there will be some variability in the interactions due to the phase of the wind fluctuations. Owing to the formulation of the idealised non-homogeneous topography and fuel beds in these simulations, there are pairs of locations (such as points 1 and 2) that have the same local and nearby fuel configurations and the same local slope. No other locations in the grid will have the same slope and fuel configuration as the points in the pair; there is not a point 3 and point 4 that are the same in both fuel and slope as points 1 and 2. There might be additional points at the same elevation that have the same slope and are 'similar' in fuel (but 'similar' is another topic for research, as mentioned above), but they would not be points that are in the same location with respect to the progressing fire (similar distance from the centreline of the progressing head fire) because the process balances near the head of the fire will not be the same as those near the flanking fire (described in Cunningham and Linn 2007). As a part of this future research, different fuel beds and topography will be used in order to allow a much larger sampling of local processes in order to construct a more complete statistical description of the evolution of the process interactions of the fire as well as the correlations between the fluctuations of various quantities.

Acknowledgements

The Los Alamos National Laboratory Institutional Computing Program provided critical computing resources for this work. Financial support for this work was provided by the USDA Forest Service's Rocky Mountain and Pacific South-west Research Stations, the Joint Fire Science program, and the National Fire Plan.

References

Anderson HE (1983) Predicting wind-driven wildland fire size and shape. USDA Forest Service, Intermountain Forest and Range Experiment Station, Research Paper INT-305. (Ogden, UT)

Andrews PL (1986) BEHAVE: Fire Behavior Prediction and Burning Modeling System – BURN subsystem, Part 1. USDA Forest Service, Intermountain Research Station, General Technical Report GTR-INT-194. (Ogden, UT)

Bossert JE, Linn RR, Reisner JM, Winterkamp JL, Dennison P, Roberts D (2000) Coupled atmosphere–fire behavior model sensitivity to spatial fuels characterization. In 'Proceedings of the Third Symposium on Fire and Forest Meteorology', January 2000, Long Beach, CA. (American Meteorological Society: Boston, MA)

Bradley M (2002) This model can take the heat. (Lawrence Livermore National Laboratory) Available at http://www.llnl.gov/str/November02/Bradley.html [Verified 24 March 2010]

Byram GM, Clements HB, Elliot ER, George PM (1964) An experimental study of model fires. USDA Forest Service, Southeastern Forest and Range Experiment Station, Project Fire Model Technical Report 3. (Asheville, NC)

Cheney NP, Gould JS, Catchpole WR (1993) The influence of fuel, weather and fire shape variables on fire-spread in grasslands. *International Journal of Wildland Fire* **3**, 31–44. doi:10.1071/WF9930031

Clark TL, Jenkins MA, Coen J, Packham D (1996) A coupled atmosphere–fire model: convective feedback on fire line dynamics. *Journal of Applied Meteorology* **35**, 875–901. doi:10.1175/1520-0450(1996)035<0875:ACAMCF>2.0.CO;2

Clark TL, Coen J, Lathan D (2004) Description of a coupled atmosphere–fire model. *International Journal of Wildland Fire* **13**, 49–63. doi:10.1071/WF03043

Coen JL (2000) Coupled atmosphere–fire model dynamics of a fireline crossing a hill. In 'Proceedings of the Third Symposium on Fire and Forest Meteorology', January 2000, Long Beach, CA. (American Meteorological Society: Boston, MA)

Cohen JD (1986) Estimating fire behavior with FIRECAST: user's manual. USDA Forest Service, Pacific Southwest Research Station, General Technical Report PSW-90. (Berkeley, CA)

Colman JJ, Linn RR (2007) Separating combustion from pyrolysis in HIGRAD/FIRETEC. *International Journal of Wildland Fire* **16**, 493–502. doi:10.1071/WF06074

Cruz MG (2004) Ignition of crown fuels above a spreading surface fire. PhD thesis, University of Montana, Missoula.

Cunningham P, Linn RR (2007) Numerical simulations of grass fires using a coupled atmosphere–fire model: dynamics of fire spread. *Journal of Geophysical Research* **112**(D05), D05108. doi:10.1029/2006JD007638

Dupuy JL (1997) Mieux comprendre et prédire la propagation des feux de forêts: expérimentation, test et proposition de modéles. PhD thesis, Université Claude Bernard, Lyon.

Dupuy JL, Larini M (1999) Fire spread through a porous forest fuel bed: a radiative and convective model including fire-induced flow effects. *International Journal of Wildland Fire* **9**, 155–172. doi:10.1071/WF00006

Dupuy JL, Morvan D (2005) Numerical study of a crown fire spreading toward a fuel break using a multiphase physical model. *International Journal of Wildland Fire* **14**, 141–151. doi:10.1071/WF04028.

Finney MA (1998) FARSITE: Fire Area Simulator – model development and evaluation. USDA Forest Service, Rocky Mountain Research Station, Paper RMRS-RP-4. (Ogden, UT)

Fons WT (1946) Analysis of fire spread in light forest fuels. *Journal of Agricultural Research* **72**, 93–121.

Forestry Canada Fire Danger Group (1992) Development and structure of the Canadian Forest Fire Behavior Prediction System. Canadian Forest Service Information Report ST-X-3. (Ottawa, ON)

Forthofer JM, Butler BW, Shannon KS, Finney MA, Bradshaw LS, Stratton R (2003) Predicting surface winds in complex terrain for use in fire spread models. In 'Proceedings of the Fifth Symposium on Fire and Forest Meteorology', November 2003, Orlando, FL. (American Meteorological Society: Boston, MA)

Grishin AM (2001*a*) Heat and mass transfer and modeling and prediction of environmental catastrophes. *Journal of Engineering Physics and Thermophysics* **74**, 895–903. doi:10.1023/A:1012394904021

Grishin AM (2001*b*) Conjugate problems of heat and mass exchange and the physicomathematical theory of forest fires. *Journal of Engineering Physics and Thermophysics* **74**, 904–911. doi:10.1023/A:1012347020859

Heilman WE (1992) Atmospheric simulations of extreme surface heating episodes on simple hills. *International Journal of Wildland Fire* **2**(3), 99–114. doi:10.1071/WF9920099

Koo E, Pagni P, Woycheese J, Stephens S, Weise D, Huff J (2005) A simple physical model for forest fire spread. In 'Fire Safety Science – Proceedings of Eighth International Symposium', 18–23 September 2005, Tsinghua University, Beijing, China. (Eds DT Gottuk, BY Lattimer) pp. 851–862. (International Association of Fire Safety Science)

Lindenmuth AW, Jr, Davis JR (1973) Predicting fire spread in Arizona's oak chaparral. USDA Forest Service, Rocky Mountain Forest and Range Experiment Station, Research Paper RM-101. (Fort Collins, CO)

Linn R, Reisner J, Colman JJ, Winterkamp J (2002) Studying wildfire behavior using FIRETEC. *International Journal of Wildland Fire* **11**, 233–246. doi:10.1071/WF02007

Linn R, Winterkamp J, Colman JJ, Edminster C, Bailey JD (2005) Modeling interactions between fire and atmosphere in discrete element fuel beds. *International Journal of Wildland Fire* **14**, 37–48. doi:10.1071/WF04043

Linn R, Winterkamp J, Edminster C, Colman JJ, Smith WS (2007) Coupled influences of topography and wind on wildland fire behaviour. *International Journal of Wildland Fire* **16**, 183–195. doi:10.1071/WF06078

Linn RR (1997) Transport model for prediction of wildfire behavior. Los Alamos National Laboratory, Scientific Report LA13334-T. (Los Alamos, NM)

Linn RR, Cunningham P (2005) Numerical simulations of grass fires using a coupled atmosphere–fire model: basic fire behavior and dependence on wind speed. *Journal of Geophysical Research* **110**(D13), D13107. doi:10.1029/2004JD005597

Mahalingam S, Zhou X, Tachajapong W, Weise DR (2005) An examination of marginal burning and transition from ground-to-crown fires using laboratory and computational modeling. In 'Proceedings of the 5th NRIFD Symposium', November 2005, Mitaka, Japan. (National Research Institute of Fire and Disaster: Japan)

Margerit J, Séro-Guillaume O (2002) Modelling forest fires. Part II: reduction to two-dimensional models and simulation of propagation. *International Journal of Heat and Mass Transfer* **45**, 1723–1737. doi:10.1016/S0017-9310(01)00249-6

Mell W, Jenkins MA, Gould J, Cheney P (2007) A physics-based approach to modeling grassland fires. *International Journal of Wildland Fire* **16**, 1–22. doi:10.1071/WF06002

Nelson RM, Jr (2002) An effective wind speed for models of fire spread. *International Journal of Wildland Fire* **11**, 153–161. doi:10.1071/WF02031

Porterie B, Morvan D, Loraud J-C, Larini M (2000) Firespread through fuel beds: modeling of wind-aided fires and induced hydrodynamics. *Physics of Fluids* **12**, 1762–1782. doi:10.1063/1.870426

Reisner JM, Bossert J, Winterkamp J (1998) Numerical simulation of two wildfire events using a combined modeling system (HIGRAD/

BEHAVE). In 'Proceedings of the Second Symposium on Fire and Forest Meteorology', January 1998, Phoenix, AZ. (American Meteorological Society: Boston, MA)

Richards GD (1990) An elliptical growth model of forest fire fronts and its numerical solution. *International Journal for Numerical Methods in Engineering* **30**, 1163–1179. doi:10.1002/NME.1620300606

Rothermel RC (1972) A mathematical model for predicting fire spread in wildland fuels. USDA Forest Service, Intermountain Forest and Range Experiment Station, Research Paper INT-115. (Ogden, UT)

Séro-Guillaume O, Margerit J (2002) Modelling forest fires. Part I: a complete set of equations derived by extended irreversible thermodynamics. *International Journal of Heat and Mass Transfer* **45**, 1705–1722. doi:10.1016/S0017-9310(01)00248-4

Tachajapong W, Zhou X, Mahalingam S, Weise DR (2006) Understanding crown fire initiation via experimental and computational modeling. In 'Proceedings of the Fifth International Conference on Fire Research', November 2006, Coimbra, Portugal. (Associação para o Desenvolvimento da Aerodinâmica Industrial: Coimbra, Portugal)

Viegas DX (2004*a*) Slope and wind effects on fire propagation. *International Journal of Wildland Fire* **13**, 143–156. doi:10.1071/WF03046

Viegas DX (2004*b*) On the existence of a steady-state regime for slope and wind-driven fires. *International Journal of Wildland Fire* **13**, 101–117. doi:10.1071/WF03008

Weise DR (1993) Modeling wind and slope-induced wildland fire behavior. PhD thesis, University of California, Berkeley.

Weise DR, Biging GS (1994) Effects of wind velocity and slope on fire behavior. In 'Fire Safety Science – Proceedings of the Fourth International Symposium', July 1994, Ottawa, Canada. pp. 1041–1051. (International Association for Fire Safety Science)

Weise DR, Zhou X, Sun L, Mahalingam S (2005) Fire spread in chaparral – 'go or no-go?' *International Journal of Wildland Fire* **14**, 99–106. doi:10.1071/WF04049

Zhou X, Weise DR, Mahalingam S (2005) Experimental measurements and numerical modeling of marginal burning in live chaparral fuel beds. *Proceedings of the Combustion Institute* **30**, 2287–2294. doi:10.1016/J.PROCI.2004.08.022

Zhou X, Mahalingam S, Weise DR (2007) Experimental study and large eddy simulation of effect of terrain slope on marginal burning in shrub fuel beds. *Proceedings of the Combustion Institute* **31**, 2547–2555. doi:10.1016/J.PROCI.2006.07.222

Manuscript received 2 August 2007, accepted 3 November 2008